Publication No. 02-173-236

EFFECT OF PARTICLE CHARACTERISTICS ON FATTY ACID FLOTATION OF FLORIDA PHOSPHATE ROCK

Volume IV – Fundamental Studies

Prepared by

UNIVERSITY OF FLORIDA
with Somasundaran, Inc.

under a grant sponsored by

April 2010

The Florida Institute of Phosphate Research was created in 1978 by the Florida Legislature (Chapter 378.101, Florida Statutes) and empowered to conduct research supportive to the responsible development of the state's phosphate resources. The Institute has targeted areas of research responsibility. These are: reclamation alternatives in mining and processing, including wetlands reclamation, phosphogypsum storage areas and phosphatic clay containment areas; methods for more efficient, economical and environmentally balanced phosphate recovery and processing; disposal and utilization of phosphatic clay; and environmental effects involving the health and welfare of the people, including those effects related to radiation and water consumption.

FIPR is located in Polk County, in the heart of the Central Florida phosphate district. The Institute seeks to serve as an information center on phosphate-related topics and welcomes information requests made in person, or by mail, email, or telephone.

Florida Institute of Phosphate Research
1855 West Main Street
Bartow, Florida 33830
(863) 534-7160
Fax: (863) 534-7165
http://www.fipr.state.fl.us

EFFECT OF PARTICLE CHARACTERISTICS ON FATTY ACID FLOTATION OF FLORIDA PHOSPHATE ROCK

FINAL REPORT

VOLUME IV
FUNDAMENTAL STUDIES

Hassan El-Shall
Principal Investigator

Department of Materials Science and Engineering
UNIVERSITY OF FLORIDA
Gainesville, FL 32611

with

P. Somasundaran
Co-Principal Investigator
SOMASUNDARAN, INC.,
Nyack, NY

Prepared for

FLORIDA INSTITUTE OF PHOSPHATE RESEARCH
1855 West Main Street
Bartow, FL 33830 USA

Project Manager: Patrick Zhang
FIPR Project Number: 05-02-173R

April 2010

DISCLAIMER

The contents of this report are reproduced herein as received from the contractor. The report may have been edited as to format in conformance with the FIPR *Style Manual*.

The opinions, findings and conclusions expressed herein are not necessarily those of the Florida Institute of Phosphate Research, nor does mention of company names or products constitute endorsement by the Florida Institute of Phosphate Research.

PERSPECTIVE

Patrick Zhang, Research Director - Beneficiation & Mining

Fatty acid flotation is the key step in phosphate beneficiation, and has significant impacts on both the operational cost and product grade. The Bone Valley phosphate deposit has been very amenable to fatty acid flotation, and is indeed one of the easiest-to-float phosphates in the world. That is changing as phosphate mining moves further south. The industry now frequently encounters difficult-to-float phosphates, with flotation recoveries 20% lower than normal. The extent of this problem and the reasons for the poor flotation performance are not understood. There has been some speculation on the cause of this problem, such as organic coating on the phosphate surfaces, higher pyrite content, and bacterial action. However, no study has been undertaken to fully investigate it.

Over the years, processing engineers within the Florida phosphate industry have urged FIPR to conduct a study of flotation feed variations to answer the question why some feeds are difficult to float, so that effective methods may be developed to improve flotation efficiency. This topic was also the only immediate research priority supported by most participants at a FIPR-sponsored flotation workshop held in 2004. In response to that top research need recommended by industry representatives, a consortium of three top universities in mineral processing/surface chemistry proposed this comprehensive study of physical, chemical, mineralogical, and surface properties of various flotation feeds to identify important parameters affecting phosphate flotation and develop methods for reducing any detrimental effects.

This characterization study used many of the routine and modern analytical techniques currently available, such as XMT, CT, XPS, CMT, FTIR, EDS and SEM. Poor flotation was found to be caused by one or more of the following characteristics:

1. Encapsulation of phosphate particles in a thin or thick silica shell

2. Heavy contamination of phosphate particles with contaminants like clay, gypsum, aluminosilicates, and dolomite

3. The presence of phosphate as coarse and/or porous particles

4. The presence of adsorption-hindering species such as silanol groups on the phosphate surface.

Although this project has not achieved the ultimate goal of instantaneous diagnostics of “bad” flotation feeds and “quick fixes” when problems are identified, this final report provides a wealth of useful information to both process engineers and researchers.

ABSTRACT

There is often considerable variation in the flotation performance of phosphate ores. There is also variation in the phosphate ore feed quality from day to day, shift to shift, and even from dragline to dragline. This study was conducted in order to determine the role of the feed variability in causing the difficulties in achieving target beneficiation with available reagents and conditions schemes. The variability of the feed can be attributed to bulk mineralogy of feed, particle size and degree of liberation of the phosphate minerals from the feed upon grinding, physicochemical properties of the phosphates minerals which dictates the optimum interaction of reagents for beneficiation. Towards identifying the critical problems, various surface and bulk characterization methodology was used: XRD analysis to obtain mineralogical properties of the liberated phosphate minerals, adsorption of reagents on the phosphate feed, zeta-potential to obtain surface charge characteristics, FTIR to identify the interaction mechanisms with reagents. It was observed that the variability in the feed was primarily due to the following factors: association of phosphate minerals with different types of silicates in varying proportions; existence of silanol groups on some of the liberated phosphate particles; presence of organic phase with some of the phosphate samples.

TABLE OF CONTENTS

LIST OF FIGURES

Figure **Page**

LIST OF FIGURES (CONT.)

LIST OF FIGURES (CONT.)

Figure **Page**

LIST OF TABLES

Table **Page**

EXECUTIVE SUMMARY

A challenging problem in phosphate beneficiation is the variability in flotation performance often due to variability in feed quality. Inasmuch as the variability of the feed may be due to variations in bulk mineralogy of feed, particle size, degree of liberation of the phosphate and physicochemical properties of the phosphates minerals, this investigation was aimed towards identifying the critical factors responsible for the poor performance of some feed.

Importantly, in order to identify such factors, good and bad flotation samples supplied by FIPR were studied using various surface and bulk characterization methodology: collector adsorption, zeta-potential measurements, x-ray fluorescence, EDX, XRD and FTIR. It was observed that the variability in the feed was primarily due to the following factors: association of phosphate minerals with different types of silicates in varying proportions; existence of silanol groups on some of the liberated phosphate particles; presence of organic phase with some of the phosphate samples.

Distinctly different in appearance, coarse black and fine black particles were hand-picked from feed, tailings, and concentrate samples and analysis was carried out using FTIR spectroscopy. It was found that the coarse black, fine black and brown pebble-like particles are phosphate mineral-bearing particles. The ratio of the carbonate (1425 cm^{-1}, 1456 cm^{-1}) to the phosphate (1030 cm^{-1}) absorption bands showed no difference among CF East tails and concentrate from good phosphate samples, suggesting no difference in the amount of carbonate substitution. However, in some FCO Bad concentrate the ratio was observed to be higher. From the comparisons of tailings and concentrate of CF East samples, tailings are characterized by a higher intensity of a band at about 3620 cm^{-1}. This band originates from the stretching vibrations of the acidic bridged hydroxyls associated with tetrahedrally coordinated framework aluminum atoms (Al T-atoms), common for the spectra of all Al-containing silicates.

Transmission and reflection spectra of a fine brown particle picked from tailings of the 1862 sample showed that, though this particle is mostly francolite in the bulk, its surface is enriched by silanol groups (a narrow band at 3745 cm^{-1}). Black particles from tailings of the CF West (good) sample was an admixture with dolomite and organic matter. Black particles from tailings of the 464-S2 samples were also an admixture with organic matter.

EDX analysis was performed on coarse/fine black and brown particles. Si and Al peaks observed in some of the EDX data indicated that these particles are phosphates with silicate inclusion. The weight fraction of silicon was found to be higher in the pebble-looking phosphate particles compared to the coarse black particles. A varying degree of silicate/aluminosilicate content was observed among the phosphate particles in the FCO Bad feed samples.

XRD results showed calcium aluminum silicate inclusions in the phosphate particles. White particles (quartz) picked up from FCO Bad tailings indicated that phosphate (francolite) is associated with quartz.

Adsorption results revealed the fact that collector (sodium oleate) adsorption is higher on the good samples (CF Combined, CF East and FCO Good) than on the bad samples (1862, 464-S2, FCO Bad and 3057). XRD of the white particles (mostly quartz) from the tails of the bad phosphate samples showed the presence of francolite in them. This indicates that phosphate is not liberated, or is finely disseminated in quartz/silicates. This will decrease the adsorption of collector, resulting in poor recovery.

Overall, the outcome of the project work can be summarized as below:

1. Phosphate particles from tails of the bad samples showed inclusions of quartz, organic matter, dolomite, and Mg and Al silicate minerals associated with phosphates. Phosphate is not completely liberated from alumosilicates and silicates, this being one of the reasons for poor flotation performance. The presence of Mg and Al silicates creates problems in metallurgical performance for various reasons, e.g., entrainment, change in pulp chemistry, rheology of the pulp.

2. Some of the samples where phosphates are lost in the tails contain organic matter. The degree of association of organic matter on the phosphate particles would determine whether collector can adsorb onto the surface.

3. Silanol groups are present on the surface of some of the phosphate tail samples.

4. Phosphate is present as fine inclusions in the silicates in a bad phosphate sample (FCO Bad). The liberation of fine phosphates will require very fine grinding. Again, fine grinding will generate various processing problems.

INTRODUCTION

BACKGROUND

Rock phosphate contains fluoroapatite/francolite along with other impurities such as quartz, clay minerals, dolomite and calcite. Separation of apatite from quartz in rock phosphates is achieved through a two-step flotation process. In this process valuable apatite is floated using an anionic surfactant such as sodium oleate, with the quartz going to the tails. To refine the concentrates that contain mostly apatite but also some amounts of quartz, it is further floated using a cationic surfactant. In this step, the quartz reports to the concentrate whereas the apatite reports to the tail. A serious problem encountered in this process is the erratic flotation performance of some feeds. This research was carried out in order to identify the reasons for such behavior. In this report, we present adsorption, XRF, XRD, FTIR and zeta potential results for different good and bad phosphate flotation product samples provided by FIPR.

OBJECTIVE

The objective of the study was to identify differences in bulk and surface properties of various flotation system components (feeds, concentrates and tailings) and delineate the factors responsible for the poor flotation and/or selectivity of some ores.

APPROACH

Owing to differences in the flotation responses of various phosphate ores, it is important to identify similarities and differences in the surface mineralogy of feeds, concentrates and tailings of phosphate samples that perform differently in flotation. Besides mineralogy, surface charge and surface contamination with other minerals can also affect the flotation behavior. EDX elemental analysis was therefore carried out along with XRF, FTIR and elctrophoretic tests in order to obtain information on the possible existence of foreign organic matter or other minerals/silicates in the micron-thick surface layer of phosphate ore particles (depending on the electron energy used, the EDX sampling depth was 1-10 μm). XRF spectrometric analysis yields a comparative estimate of key elements in the bulk of the particles, since the XRF sampling depth is 1-10 mm. Electrophoretic measurements yield data on surface charge. FTIR microscopy measurements in the transmission and reflection modes provide information about bulk and surface (several-micron thick) structure of the particles, respectively, which is complementary to the EDX, XRD and XRF data. Sodium oleate is used as a collector in the selective recovery of phosphate. Hence, the adsorption behavior of sodium oleate on different phosphate feed samples was also investigated.

MATERIALS AND EXPERIMENTAL PROCEDURE

MATERIALS

Initially four feed samples (FCO Good and Bad and CF Good and Bad) were received. Thirty-three different phosphate samples were also obtained from FIPR. They were grouped as Four Corners Bad feed, Hole 1862 Split 2 (1862-S2), Hole 464 Split 2 (464-S2), Hole 464 Split 1 (464-S1), CF East Pit, CF West Pit, CF Combined, Hole 3057, FCO 5-2-07 and SFM. Feed, concentrate and tailings were available for each of these groups. Samples provided for analysis showed varying degrees of flotation response. As per the objective presented earlier, the samples were sub-grouped into good and bad samples. Feeds, concentrates and tailings from the good and bad sub-groups were selected for different surface experiments and their results were compared for differences in surface properties. In this report CF East, CF West, CF Combined and FCO Good (FCO 5/2/07) are reported as the good samples; FCO Bad, 1862-S2, 464-S1 and 464-S2, and 3057-S2, SFM are reported as the bad samples.

EDX METHODOLOGY

Energy dispersive X-ray analysis (EDX) was performed on the feed sample of the FCO Bad sample. In this feed sample, black and brown particles suspected to be phosphates were picked out and EDX experiments were performed on these individual particles. A Princeton Gamma Tech instrument was used for this purpose.

XRF ANALYSIS

XRF elemental analysis on selected phosphate samples was carried out with an Innovxsystems XRF spectrometer. A phosphate sample of desired quantity was placed in the sample cup holder. The instrument mode was in the soil mode and tests were carried out in triplicate and averaged. Each sample was analyzed for 60 seconds. The instrument does not provide quantitative surface elemental composition if it exceeds 10% of the total surface area.

ADSORPTION EXPERIMENTS

High-purity sodium oleate was obtained from Pfaltz & Bauer, Inc. A 5000 ppm stock solution of sodium oleate was prepared using triple distilled water. This stock solution was further diluted to appropriate values to determine the reagent concentration effect on the adsorption on the two samples. The critical micelle concentration (CMC) of the sodium oleate surfactant is 0.00090 M. Both good feed (CF East and FCO Good) and bad feed (1862 and 464) samples were studied at initial reagent concentrations of 0, 25, 50, 100, 200, 500, 1000, and 2000 ppm. Adsorption experiments were conducted in 10

ml vials. Solid 1 gm samples were mixed with 5 ml of triple distilled water and conditioned for 2 hours at room temperature. The pH of the triple distilled water was adjusted to pH 9.3 with NaOH. Further, 5 ml of the surfactant solution (prepared with triple distilled water at pH 9.2) was added and the samples were equilibrated for 3 hours, then centrifuged for 30 min at 5000 rpm. The clear supernatant was then pipetted out for analysis. The surfactant depletion from the solutions yields the amount of adsorption as a function of the residual surfactant concentrations. A Shimadzu TOC-5000A total carbon analyzer was used to determine the total organic carbon present in the residual surfactant supernatant. Adsorption tests on CF Combined, 3057 and FCO Bad samples were carried out with the above-mentioned procedure, except that the samples were equilibrated for 18 hours instead of 3 hours.

Duplicate tests were performed for a few of the reagent concentrations.

ZETA POTENTIAL STUDIES

Zeta potential studies were carried out on feed samples of FCO and CF received at the beginning of the project. Zeta potential studies were also performed with feed samples (CF East feed, FCO 5-07 and CF Combined) and feed (1862, FCO Bad, 3057) samples which had reportedly shown good and bad flotation, respectively. Electrophoretic tests were also performed on tailings to obtain an insight into their interfacial behavior. The desired amounts of samples were added to triple distilled water and the pH was adjusted using 0.2M HCl and 0.2M NaOH. The samples were sonicated and equilibrated for 12 hours. The supernatant was used to study the zeta potential of the samples using a Zeta meter 2.0 instrument.

XRD ANALYSIS

Coarse and fine black particles (phosphates) and white particles (quartz) were handpicked and analyzed for mineralogy using XRD. X-ray diffractograms were taken using a Rijaku X-ray powder diffractometer. A CuKα (λ = 0.154 nm) radiation source operated at 40 kV and 40 mA was used. Twenty to forty particles from respective samples were placed on a zero background plate for XRD measurements.

FTIR STUDY

From one to four coarse/fine sized black and brown particles were separated from concentrates and tailings of different samples (CF East, CF West, 464, 1862, SFM, 3057-S2, and FCO Bad). These samples were chosen as they have shown varying degrees of recovery, good as well as bad. FTIR spectra were measured for various particles, separated using a FTIR microscope and spectra developed in both the attenuated total reflectance (ATR) and transmission modes. To distinguish the differences between the surface and bulk of the particles, spectra were collected in both the attenuated total

reflectance (ATR) and transmission modes at spectral resolution of 4 cm^{-1} and the number of scans was 256. The former technique is more sensitive to the particle surface, while the latter provides absorption spectra of the whole particle and has a much higher signal-to-noise ratio in the 4000-2000-cm^{-1} region, where stretching vibrations of the surface and bulk hydroxyl groups and surface silanol and aluminol groups are active. In most cases, both ATR and transmission were measured on the same particle. The number of particles analyzed varied from 3 to 5. In addition, FTIR diffuse reflectance spectra were measured on ground fine black particles picked from tailings of FCO Bad samples to understand the surface-bulk partitioning of phosphate inclusions.

RESULTS AND DISCUSSION

EDX ANALYSIS

EDX data for FCO Bad and FCO Good feed samples were analyzed and a few representative results are presented in Figures 1 to 7, along with the corresponding spectra for calcium, phosphorus, carbon, oxygen, fluorine, silicon, and magnesium peaks. For pure fluorapatite, the mineral Ca/P ratio (by weight) is around 2.1 (stochiometrically). It can be seen that Ca/P ratio (by weight) does vary. The presence of carbon in substantial concentration is also observed from the spectra. Based on the EDX and FTIR (given in the following sections) data available, it is suggested that a polymorph of apatite such as francolite is present in the particles studied. However, the numerical values of the carbon and oxygen shown in these spectra are not precise since the EDX instrument does not accurately differentiate the counts for carbon and oxygen. Further, magnesium was also present in all the EDX spectra reported here (Figures 1-7). Because of the presence of silicon/aluminium peaks in most of the black/brown-like particles' EDX spectra, we propose that silicates/alumina/aluminosilicates are also present in these particles (Figures 4, 6 and 7).

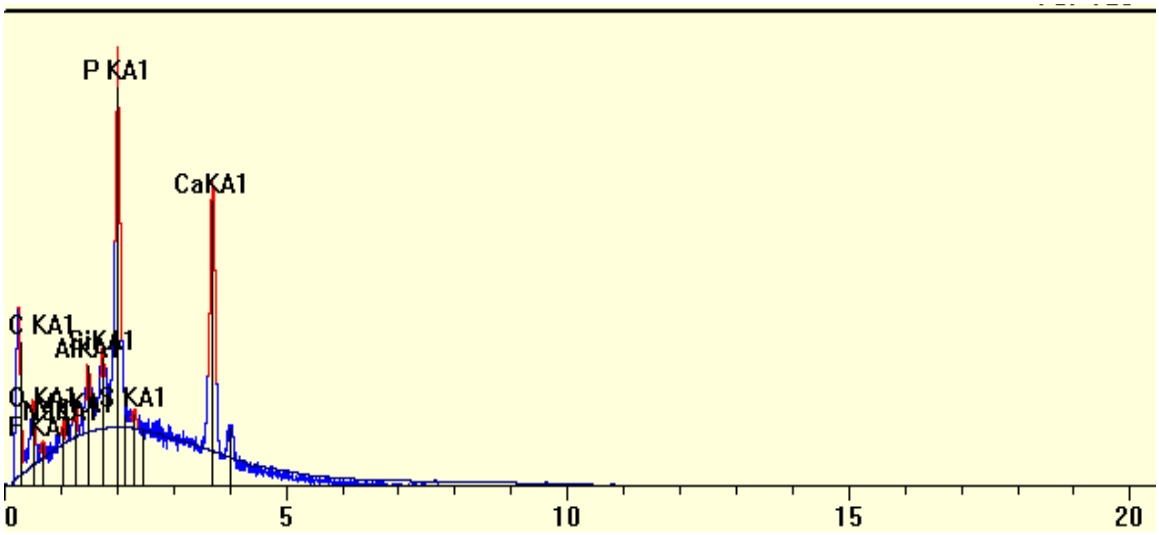

Element	Line	keV	KRatio	Wt%	At%	At Prop	ChiSquared
C	KA1	0.277	0.1112	67.03	79.82	0.0	17.67
Al	KA1	1.487	0.0094	1.27	0.68	0.0	4.19
Si	KA1	1.740	0.0129	1.58	0.80	0.0	4.19
Ca	KA1	3.691	0.0695	8.09	2.89	0.0	6.89
Mg	KA1	1.254	0.0031	0.47	0.27	0.0	4.19
O	KA1	0.523	0.0171	11.86	10.60	0.0	17.67
P	KA1	2.013	0.0596	7.44	3.44	0.0	4.19
Na	KA1	1.041	0.0032	0.63	0.39	0.0	4.19
F	KA1	0.677	0.0027	1.25	0.94	0.0	17.67
S	KA1	2.307	0.0029	0.39	0.17	0.0	4.19
Total			0.2916	100.00	100.00	0.0	5.97

Figure 1. EDX Spectrum and Percentage Analysis of Elements from FCO Feed Sample (Black Particles 1).

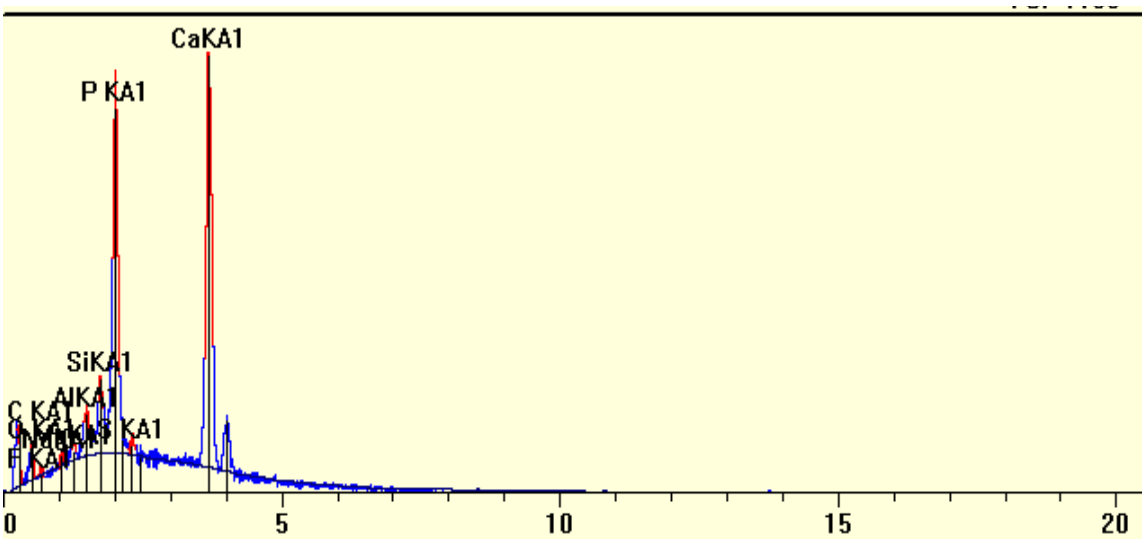

Element	Line	keV	KRatio	Wt%	At%	At Prop	ChiSquared
C	KA1	0.277	0.0766	48.46	68.18	0.0	8.56
Al	KA1	1.487	0.0126	1.67	1.05	0.0	5.09
Si	KA1	1.740	0.0209	2.47	1.49	0.0	5.09
Ca	KA1	3.691	0.1881	21.11	8.90	0.0	14.31
Mg	KA1	1.254	0.0041	0.62	0.43	0.0	5.09
O	KA1	0.523	0.0154	11.24	11.87	0.0	8.56
P	KA1	2.013	0.1075	12.93	7.05	0.0	5.09
Na	KA1	1.041	0.0024	0.48	0.35	0.0	5.09
F	KA1	0.677	0.0008	0.39	0.35	0.0	8.56
S	KA1	2.307	0.0048	0.62	0.33	0.0	5.09
Total			0.4331	100.00	100.00	0.0	7.20

Figure 2. EDX Spectrum and Percentage Analysis of Elements from FCO Feed Samples (Black Particles 2).

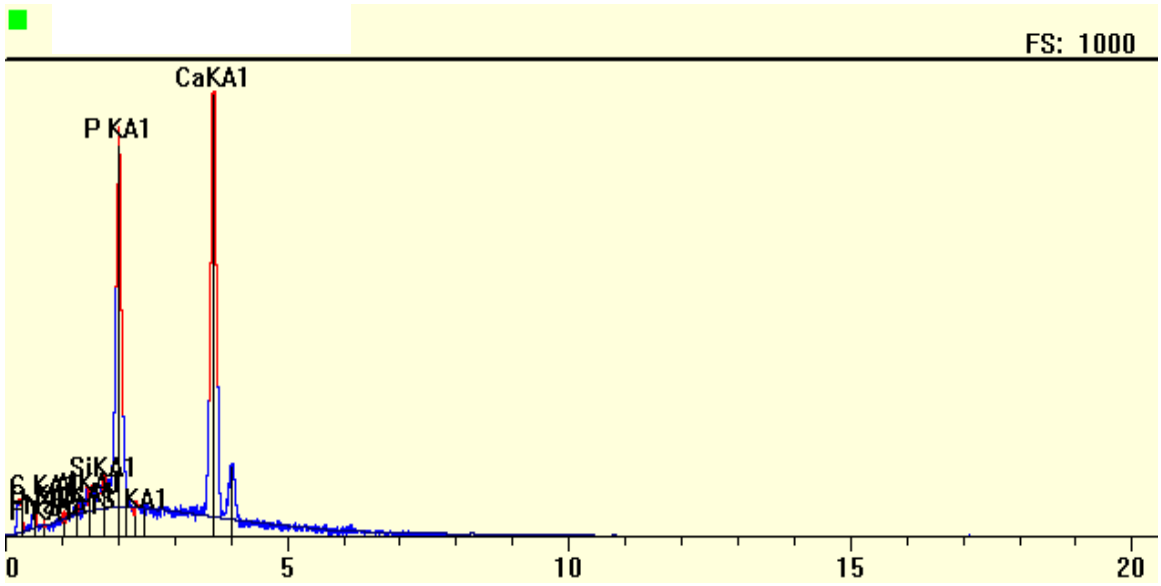

Element	Line	keV	KRatio	Wt%	At%	At Prop	ChiSquared
C	KA1	0.277	0.0639	31.29	53.57	0.0	4.35
Al	KA1	1.487	0.0092	1.27	0.97	0.0	6.26
Si	KA1	1.740	0.0135	1.62	1.18	0.0	6.26
Ca	KA1	3.691	0.3111	35.45	18.19	0.0	14.89
Mg	KA1	1.254	0.0019	0.31	0.26	0.0	6.26
O	KA1	0.523	0.0126	9.42	12.10	0.0	4.35
P	KA1	2.013	0.1722	20.56	13.65	0.0	6.26
Na	KA1	1.041	0.0004	0.08	0.07	0.0	6.26
F	KA1	0.677	0.0000	0.01	0.02	0.0	4.35
S	KA1	2.307	0.0000	0.00	0.00	0.0	
Total			0.5848	100.00	100.00	0.0	8.18

Figure 3. EDX Spectrum and Percentage Analysis of Elements from FCO Feed Sample (Black Particles 3).

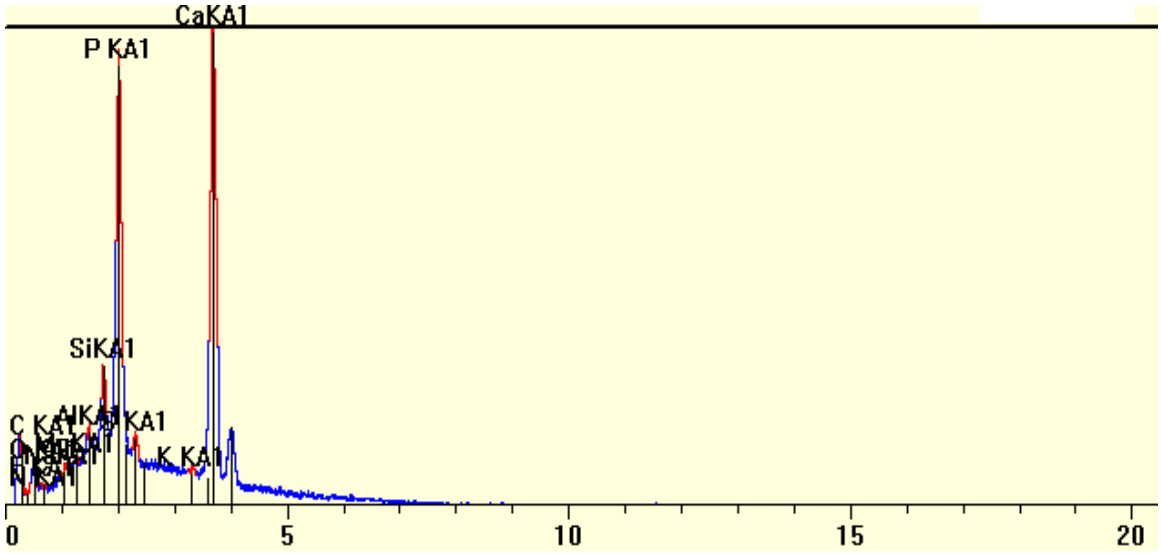

Element	Line	keV	KRatio	Wt%	At%	At Prop	ChiSquared
S	KA1	2.307	0.0068	0.89	0.47	0.0	8.24
P	KA1	2.013	0.1069	12.80	7.01	0.0	8.24
O	KA1	0.523	0.0133	9.82	10.41	0.0	14.46
Al	KA1	1.487	0.0090	1.20	0.75	0.0	8.24
Si	KA1	1.740	0.0227	2.66	1.60	0.0	8.24
Ca	KA1	3.691	0.1873	21.01	8.89	0.0	17.06
C	KA1	0.277	0.0693	44.37	62.68	0.0	14.46
N	KA1	0.392	0.0039	5.84	7.08	0.0	14.46
F	KA1	0.677	0.0011	0.50	0.45	0.0	14.46
Mg	KA1	1.254	0.0031	0.47	0.33	0.0	8.24
K	KA1	3.313	0.0000	0.00	0.00	0.0	
Na	KA1	1.041	0.0022	0.44	0.33	0.0	8.24
Total			0.4256	100.00	100.00	0.0	10.54

Figure 4. EDX Spectrum of Big Particles (FCO Feed).

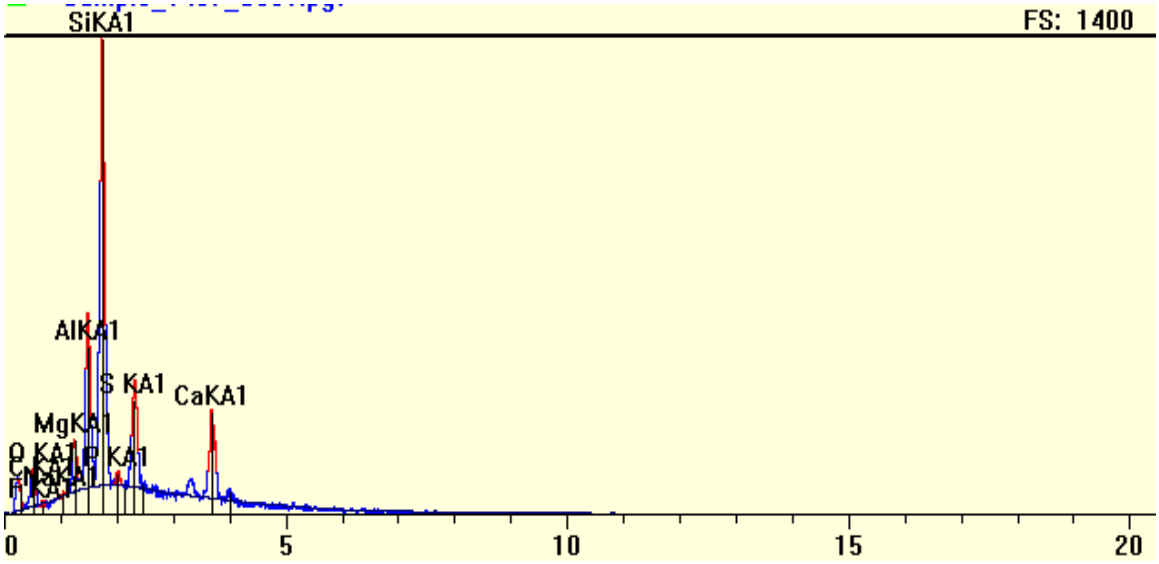

Element	Line	keV	KRatio	Wt%	At%	At Prop	ChiSquared
C	KA1	0.277	0.1027	66.09	80.26	0.0	53.00
Al	KA1	1.487	0.0077	1.02	0.55	0.0	8.28
Si	KA1	1.740	0.0458	5.50	2.85	0.0	8.28
Ca	KA1	3.691	0.0867	10.05	3.66	0.0	21.47
Mg	KA1	1.254	0.0028	0.42	0.25	0.0	8.28
O	KA1	0.523	0.0141	9.88	9.00	0.0	53.00
P	KA1	2.013	0.0483	6.46	3.04	0.0	8.28
Na	KA1	1.041	0.0010	0.19	0.12	0.0	8.28
F	KA1	0.677	0.0006	0.26	0.20	0.0	53.00
S	KA1	2.307	0.0009	0.13	0.06	0.0	8.28
Total			0.3106	100.00	100.00	0.0	14.31

Figure 5. EDX Spectra of Pebble Particle (FCO Bad Feed).

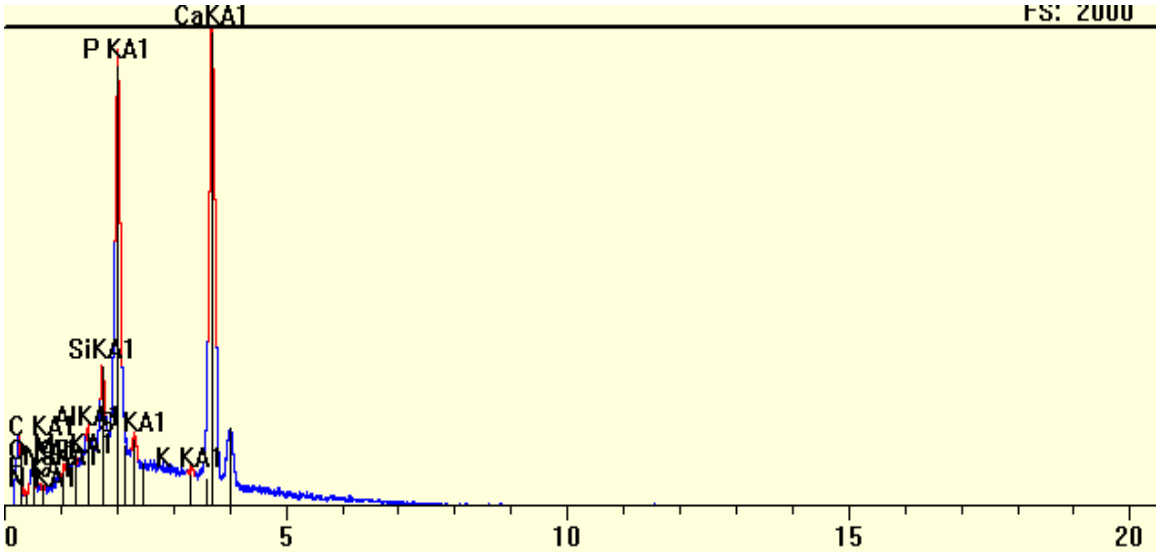

Element	Line	keV	KRatio	Wt%	At%	At Prop	ChiSquared
S	KA1	2.307	0.0068	0.89	0.47	0.0	8.24
P	KA1	2.013	0.1069	12.80	7.01	0.0	8.24
O	KA1	0.523	0.0133	9.82	10.41	0.0	14.46
Al	KA1	1.487	0.0090	1.20	0.75	0.0	8.24
Si	KA1	1.740	0.0227	2.66	1.60	0.0	8.24
Ca	KA1	3.691	0.1873	21.01	8.89	0.0	17.06
C	KA1	0.277	0.0693	44.37	62.68	0.0	14.46
N	KA1	0.392	0.0039	5.84	7.08	0.0	14.46
F	KA1	0.677	0.0011	0.50	0.45	0.0	14.46
Mg	KA1	1.254	0.0031	0.47	0.33	0.0	8.24
K	KA1	3.313	0.0000	0.00	0.00	0.0	
Na	KA1	1.041	0.0022	0.44	0.33	0.0	8.24
Total			0.4256	100.00	100.00	0.0	10.54

Figure 6. EDX Spectrum of FCO Feed (Big Black Particles).

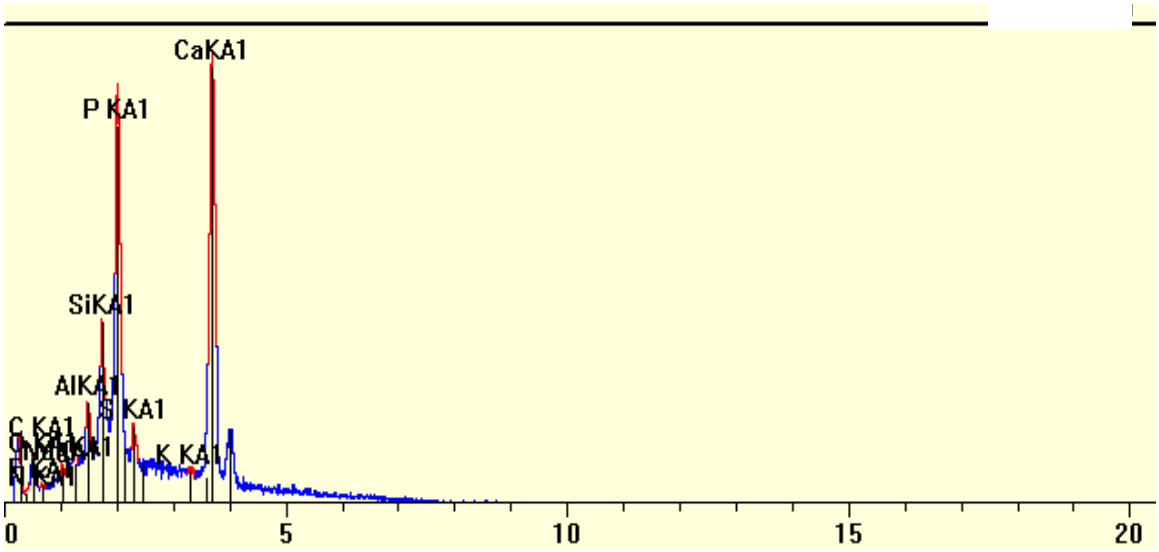

Element	Line	keV	KRatio	Wt%	At%	At Prop	ChiSquared
S	KA1	2.307	0.0024	0.27	0.18	0.0	10.46
P	KA1	2.013	0.1714	18.56	12.58	0.0	10.46
O	KA1	0.523	0.0200	6.17	8.09	0.0	23.07
Al	KA1	1.487	0.0115	1.29	1.00	0.0	10.46
Si	KA1	1.740	0.0237	2.48	1.85	0.0	10.46
Ca	KA1	3.691	0.3524	38.37	20.10	0.0	25.21
C	KA1	0.277	0.1158	29.40	51.40	0.0	23.07
N	KA1	0.392	0.0053	2.71	4.06	0.0	23.07
F	KA1	0.677	0.0014	0.32	0.36	0.0	23.07
Mg	KA1	1.254	0.0019	0.22	0.19	0.0	10.46
K	KA1	3.313	0.0000	0.00	0.00	0.0	
Na	KA1	1.041	0.0016	0.22	0.20	0.0	10.46
Total			0.7074	100.00	100.00	0.0	14.60

Figure 7. EDX of Silicates Taken from the FCO Bad Feed Sample.

XRF Analysis

XRF analysis was carried out on good (CF East Pit, FCO Good) and bad samples (FCO Bad, 1862, 464-S1) to obtain elemental analyses of such different phosphate ore samples. Owing to the importance of the comparative content of phosphorus and calcium, concentrations of other elements are not presented here. From Table 1 it can be seen that among the feed and tail samples considered for analysis, Ca percentage is high in the 1862 phosphate feed samples.

Table 1. Ca and P Concentration (ppm) in Phosphate Samples Using XRF.

	Ca Conc. (ppm)	P Conc. (ppm)
CF East Tails	6608	6765
CF East Feed	66650	13220
FCO Bad Tails	8907	7320
FCO Feed	81084	19115
FCO Bad Feed	35952	10241
1862 Split F	>10%	65653
1862 Split C	>10%	35097
1862 Split T	>10%	58578
1862 Split F	>10%	49528
464 Split1 F	82064	24775
464 Split1 T	6730	7908
464 Split1 C	>10%	78712

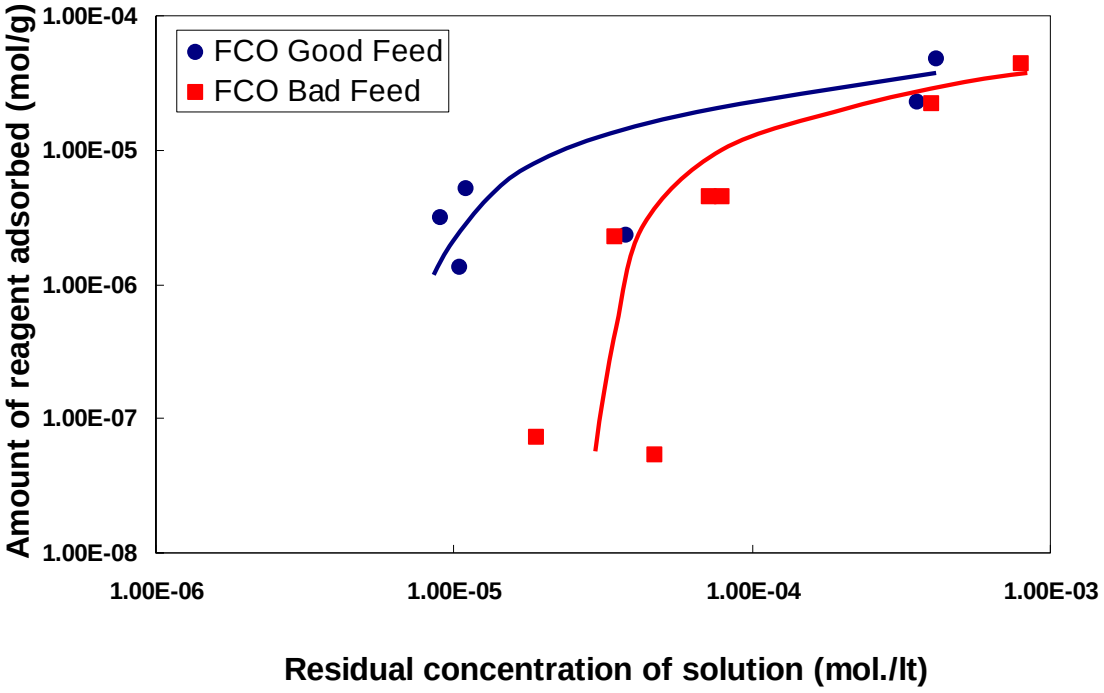

Figure 8. Adsorption Density of Sodium Oleate on Both Good and Bad Feed Samples of FCO Rock Phosphate Source at Natural pH.

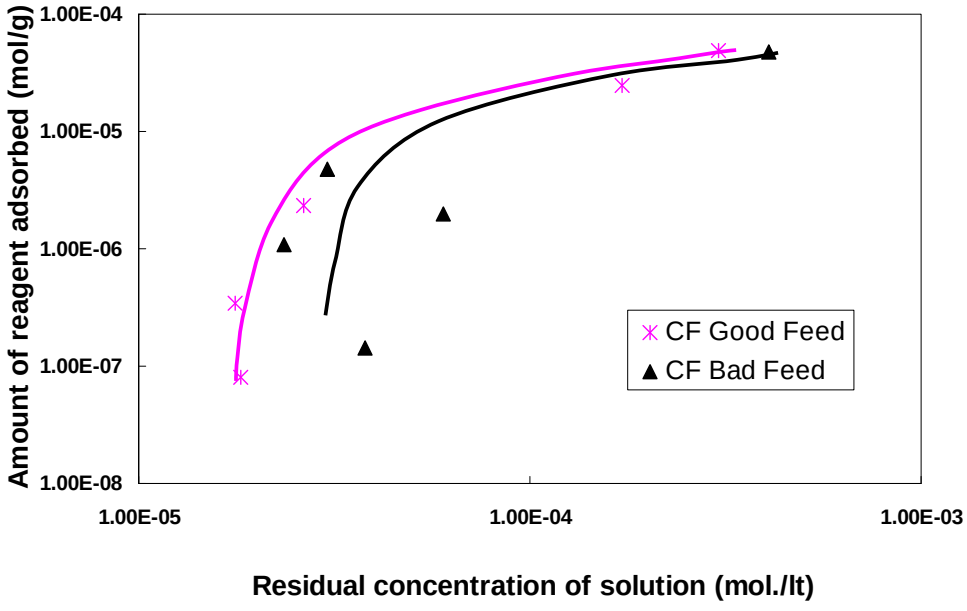

Figure 9. Adsorption Density of Sodium Oleate on Both Good and Bad Feed Samples of CF Rock Phosphate Source at Natural pH.

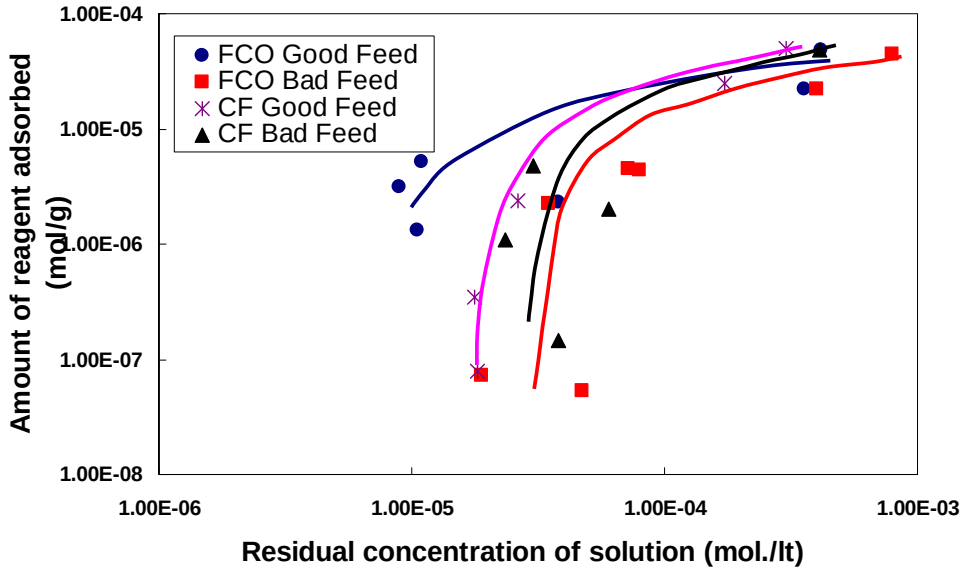

Figure 10. Adsorption Density of Sodium Oleate on Both Good and Bad Feed Samples of FCO, CF Rock Phosphate Sources at Natural pH.

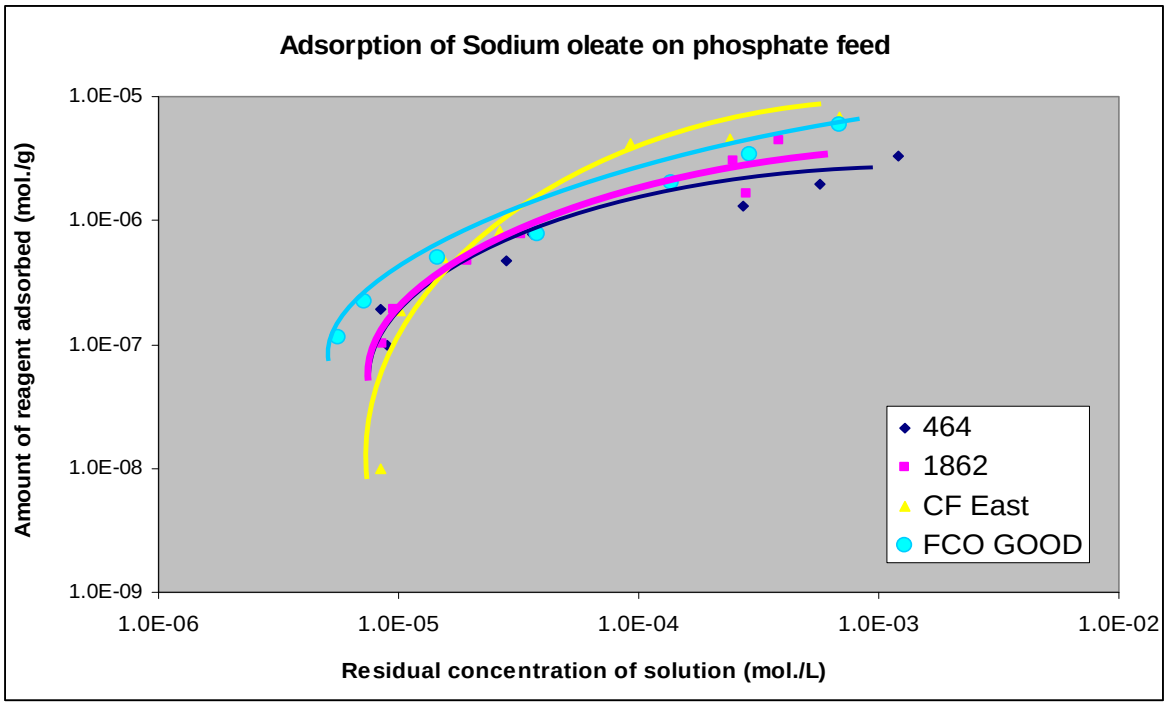

Figure 11. Adsorption Density of Sodium Oleate on Both Good (CF East, FCO 5/2/07) and Bad (1862 and 464-S1) Feed Samples at pH 9.2.

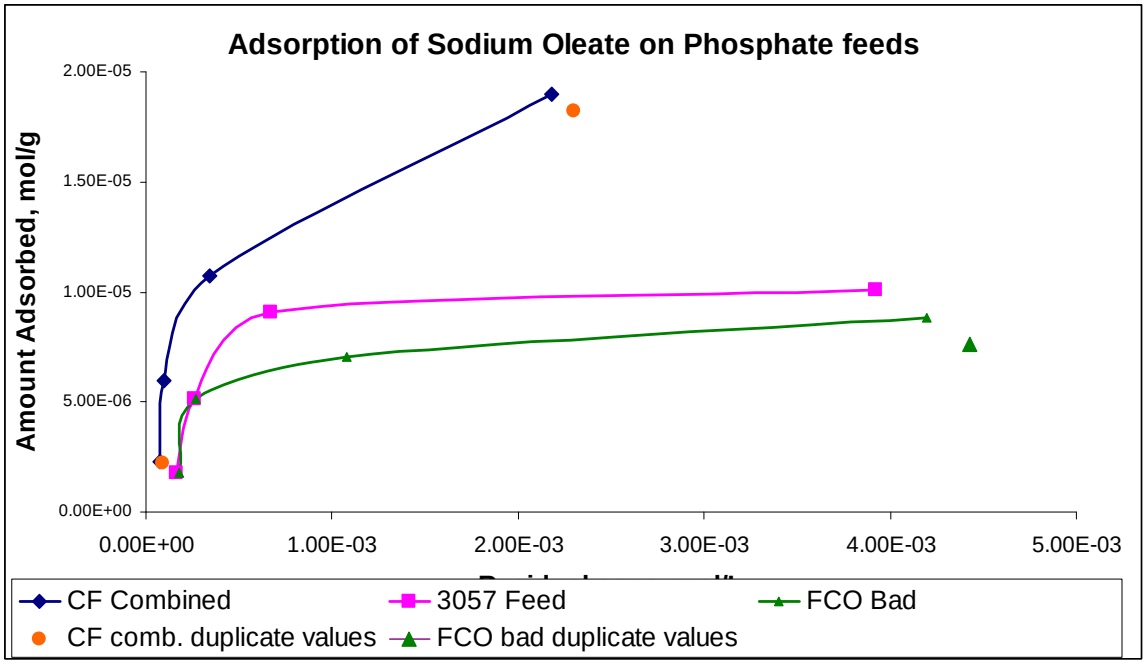

Figure 12. Adsorption Density of Sodium Oleate on Both Good (CF Combined) and Bad (3057 and FCO Bad) Feed Samples at pH 9.2.

ADSORPTION EXPERIMENTS

The results of the adsorption experiments are plotted in Figures 8 to 12. These figures show that there is very little difference between any of these samples in their adsorption characteristics of oleate. In Figures 8 to 10, the differences between the good and bad feed types can be clearly seen for oleate dosage at starvation quantities. Further, it can be noted that FCO Good feed shows better adsorption characteristics as compared to any other feed sample in low oleate concentrations. In Figures 11-12, it can be clearly seen that adsorption of sodium oleate on good samples (CF and FCO Good) is slightly higher compared to that on the 1862 and 464 samples at higher oleate dosages. In Figure 12 it can be observed that the adsorption of collector is significantly high on good phosphate samples (CF Combined), than that on the 3057 and FCO Bad phosphate samples. It was observed from the XRD data that phosphate is present in the quartz (particles picked up from tails) samples in the bad feeds (FCO Bad, see Figure 23c). This indicates that phosphate is not completely liberated from the bad feeds, and hence, this is proposed to be one of the reasons for the decrease in the adsorption of collector.

ZETA POTENTIAL

The results of these experiments are shown in Figures 13 to 22. In Figure 13, the finer particles from the concentrates show a positive charge at low pH, which decreases with the addition of alkali, yielding an isoelectric point of pH 7.2. Since the

measurement procedure takes into account only the fine particles in the system and is not a representative of complete mineral sample, it was discarded after discussions. Nevertheless, the studies would be useful for comparison with the ground concentrates. It can be seen from Figures 14 and 15 that, for both good and bad feed, the zeta potential is negative in the acidic pH range and increases slightly as the pH increases. These studies were repeated to confirm that the trend of increasing zeta potential is not an experimental artifact. The pH dependence of zeta potential is unusual and suggests pH-dependent adsorption of dissolved species such as calcium, but this is speculation at this point and has to be investigated further. This must also be explored due to its practical implications.

Figure 16 shows that both CF East feed and CF Combined feed showed similar trends in the zeta potential values. This indicates a similarity in the phosphate mineralogy, with the assumption that the effects of other family minerals have a similar contribution to zeta potential values. It should be noted that both these type of minerals showed similar behavior in terms of flotation recovery. But there is marked difference in the zeta potential of good (CF East feed and FCO 5-07) and bad feed (1862-S2) sample, as seen in Figure 17. This suggests that this sample (1862) contains apatite with mineral inclusions not common to good samples studied so far. The surface elemental composition of this sample (1862) in particular showed significant amounts of surface Ca concentration compared to the other samples studied. However, it is interesting to note that tailings of good and bad samples showed similar zeta potential results (Figure 18). XRD and FTIR analysis showed that tailings samples have a significant admixture of different silicates and organic matter. This explains why the zeta potential of the tails are of a similar nature. It can be observed from Figure 22 that 3057 has a slightly different zeta potential trend compared to other minerals. This is again due to the different mineralogy specific to this sample, in terms of association of phosphate minerals with various silicates and dolomite.

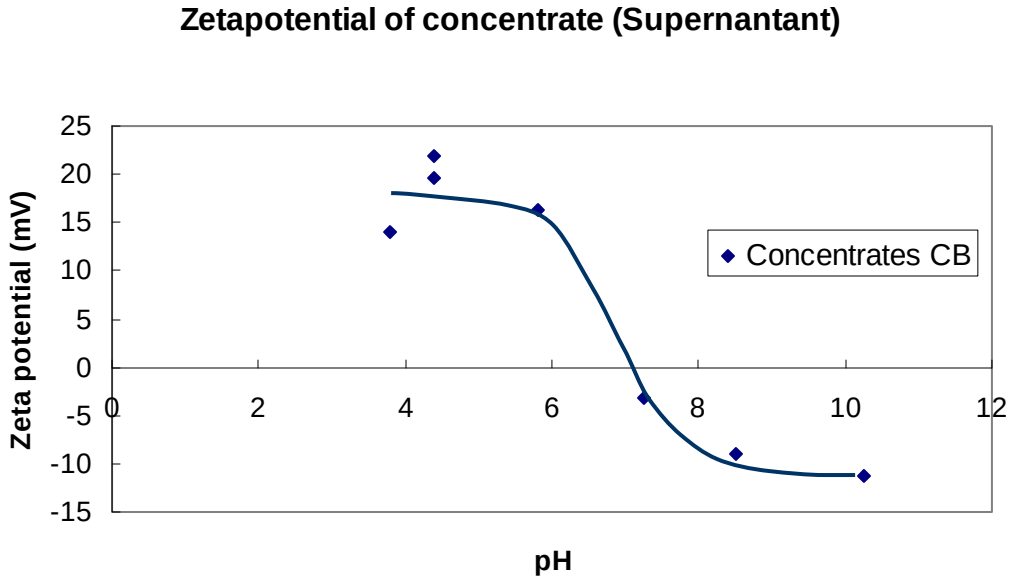

Figure 13. Zeta Potential of Concentrates (C_b) from the Flotation Experiment as a Function of pH.

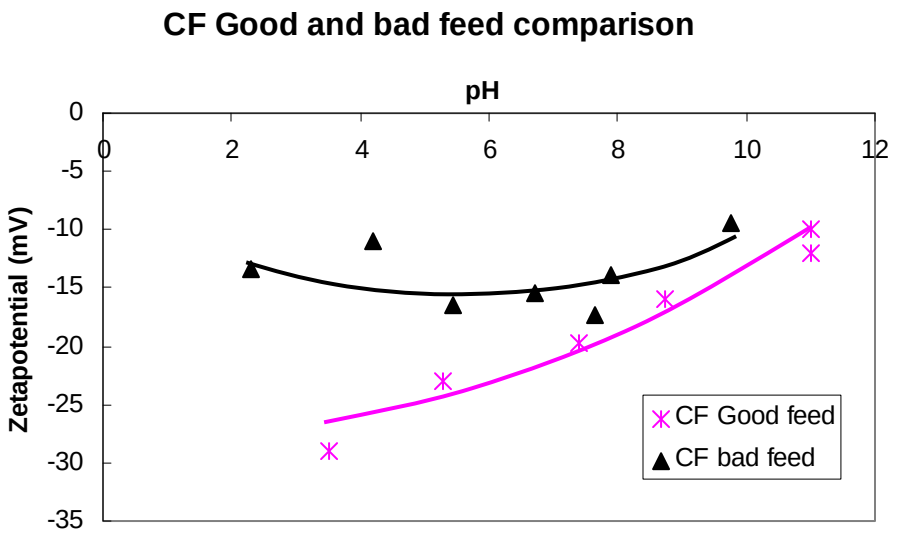

Figure 14. Zeta Potential Studies of CF Feed as a Function of pH.

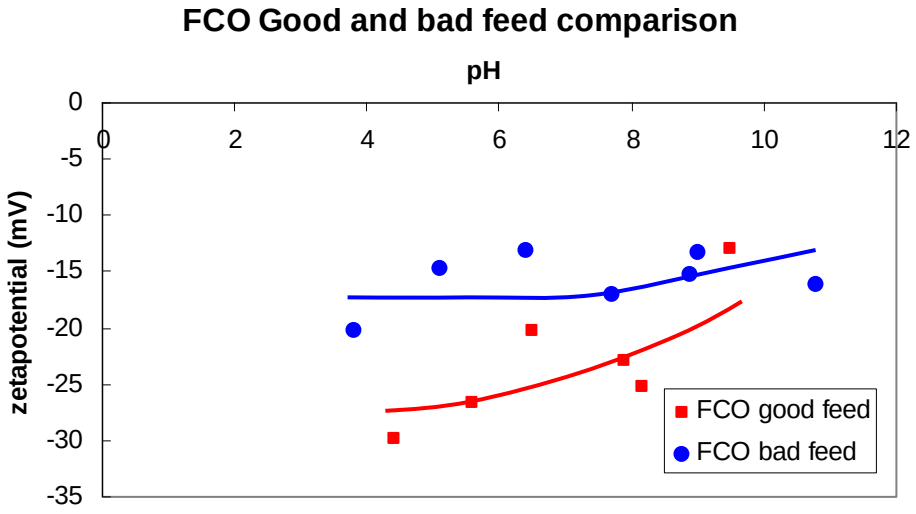

Figure 15. Zeta Potential Studies of FCO Feeds as a Function of pH.

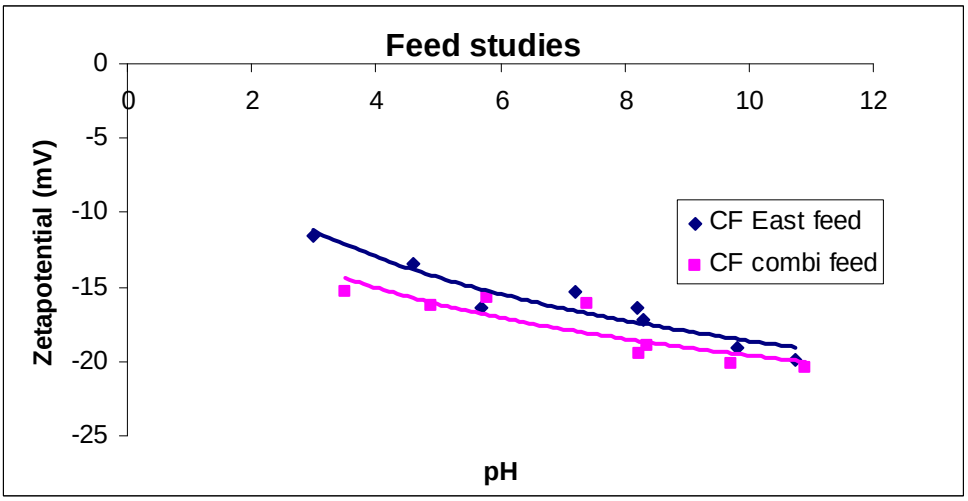

Figure 16. Zeta Potential of Phosphate Samples (CF East Feed and CF Combined Feed).

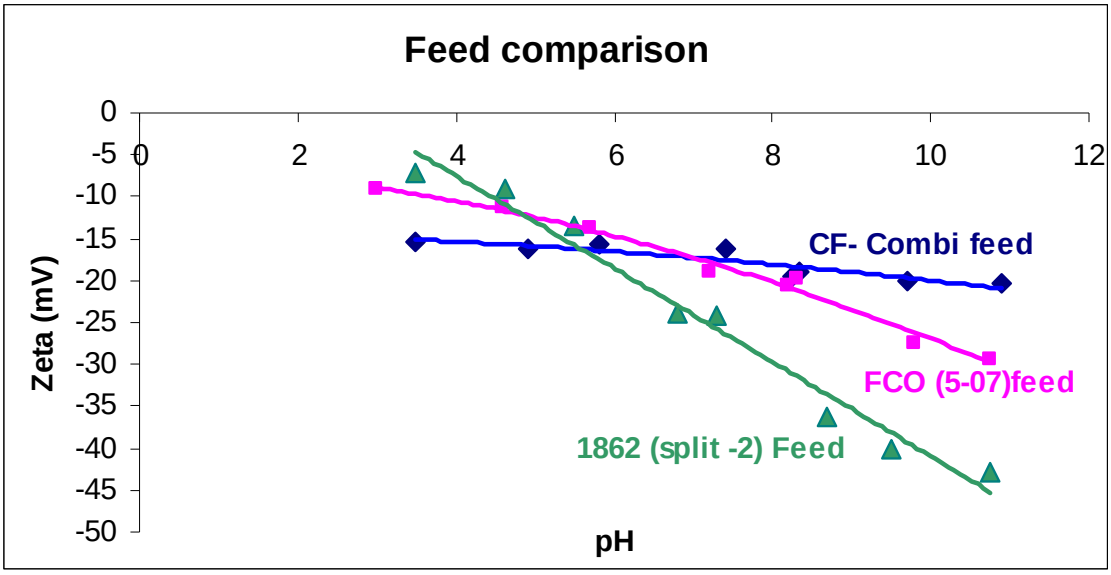

Figure 17. Zeta Potential of Phosphate Samples (FCO 5-07, 1862-S2 and CF Combined Feed).

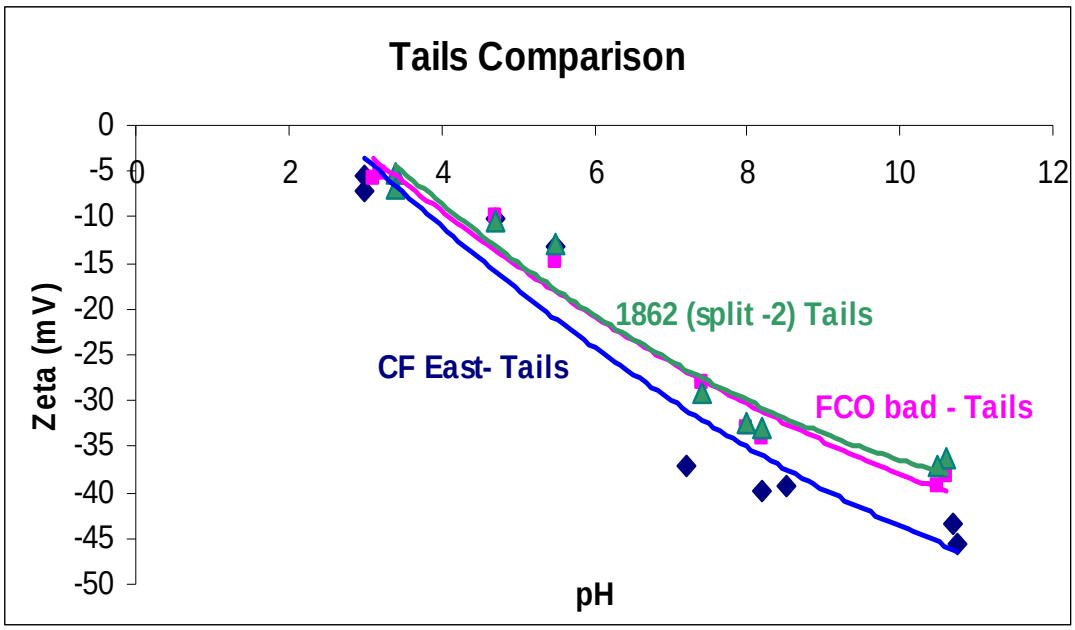

Figure 18. Zeta Potential of Phosphate Samples (FCO Bad, 1862-S2, and CF Combined Tails).

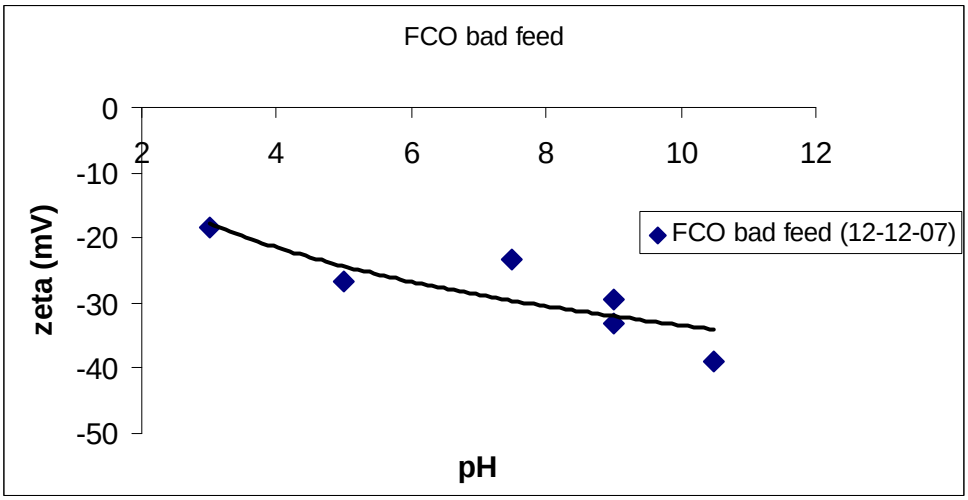

Figure 19. Zeta Potential of Phosphate Samples (FCO Bad Feed).

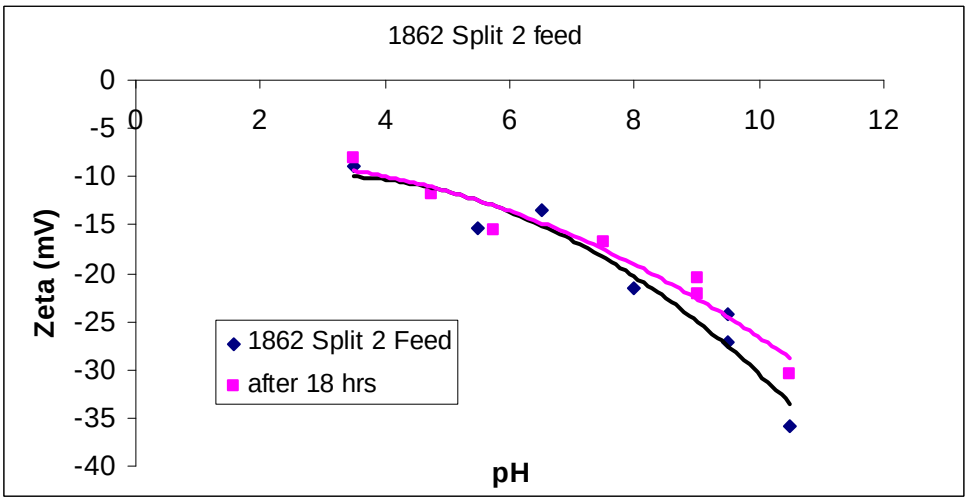

Figure 20. Zeta Potential of Phosphate Samples (1862-S2 After Different Equilibration Time).

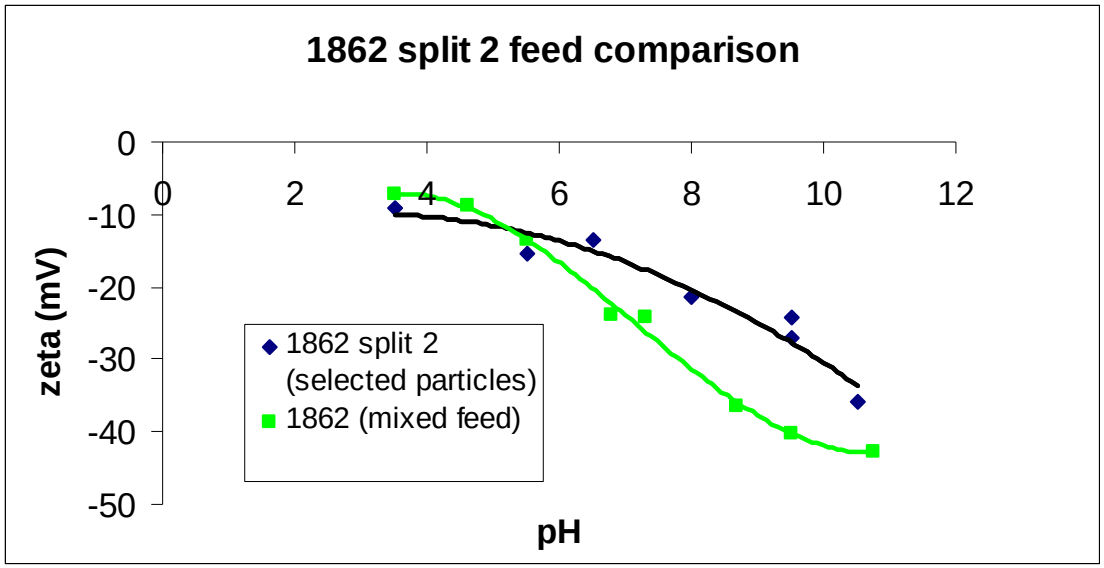

Figure 21. Zeta Potential of Phosphate Samples (Comparison of Zeta Potential of Feed as Received and Black Phosphate Particles Selected from the Feed).

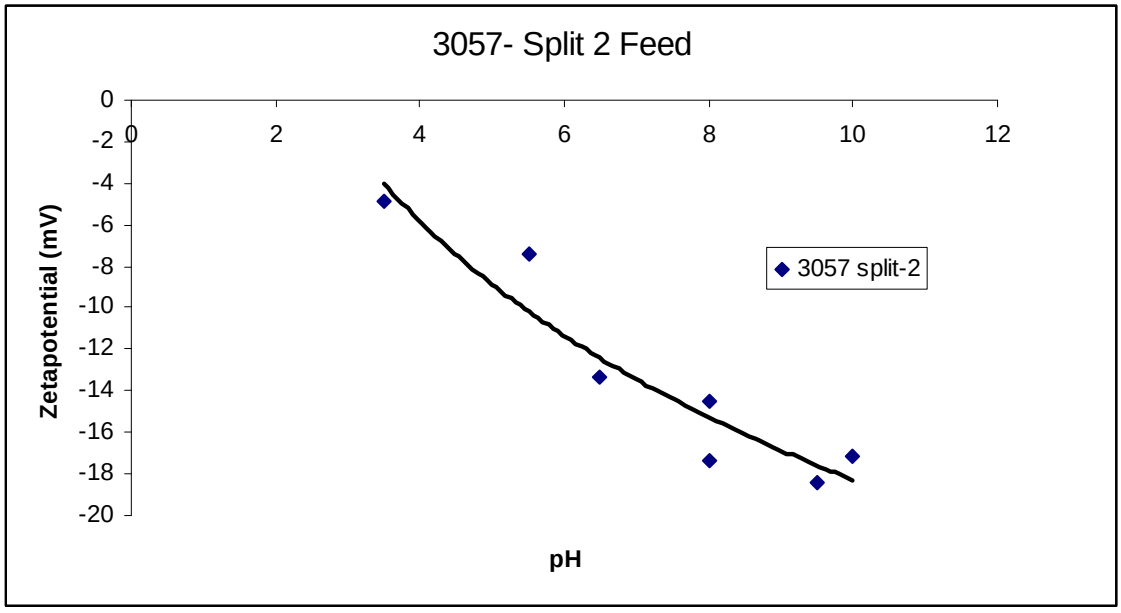

Figure 22. Zeta Potential of Phosphate Samples (3057).

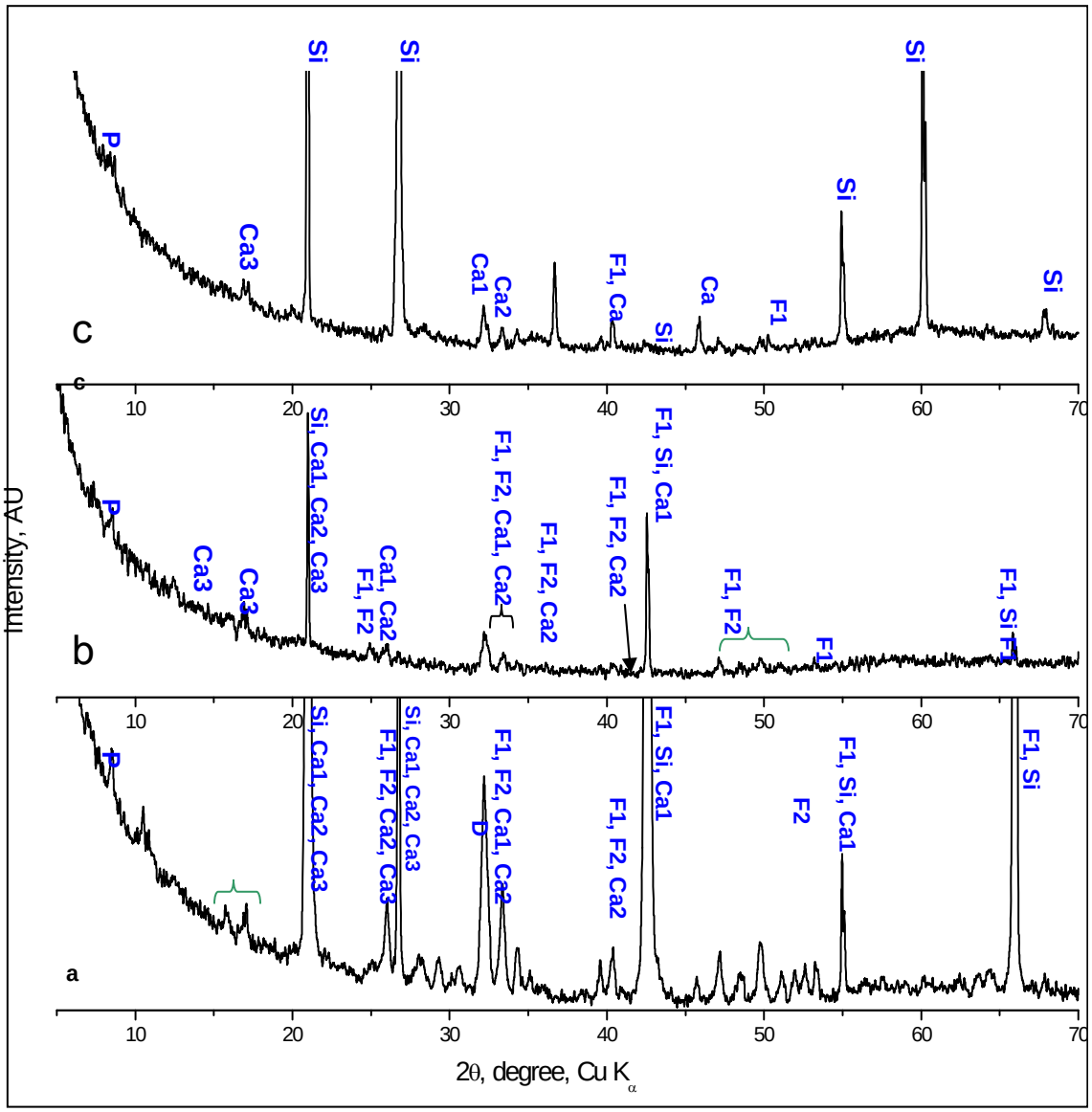

Figure 23. XRD Patterns of Particles from Tailings of FCO Bad Sample (a) Fine Black Particles; (b) Ground Coarse Black Particles; (c) White Particles.

Note: F1 = Francolite $CaF(Ca,C)_4[(P,C)(O,OH,F)_4]_3$ JCPDS 02-0833
F2 = Carbonatehydroxyapatite $Ca_{10}(PO_4)_3(CO_3)(OH)_2$ JCPDS 19-0272 or Calcium Carbonate Hydrate JCPDS 83-1923
P = Palygorskite $MgAlSi_4O_{10}(OH).4H_2O$ JCPDS 29-0855; 31-0783
C = Cordierite $Mg5(Si,Al)8O_20(OH)_2.8H_2O$ JCPDS 86-1550; 85-1722
Ca1 = Calcium Aluminum Silicate Hydrate $CaAl_2Si_2O_8.4H_2O$ JCPDS 20-0452
Ca2 = Calcium Aluminum Silicate Hydrate $CaAl_2Si_2O_8.4H_2O$ JCPDS 39-1373
Ca3 = Calcium Aluminum Silicate Hydrate $CaAl_2Si_2O_8.4H_2O$ JCPDS 13-0495
Si = Quartz
D = Dolomite $CaMg(CO_3)_2$ JCPDS 79-1346

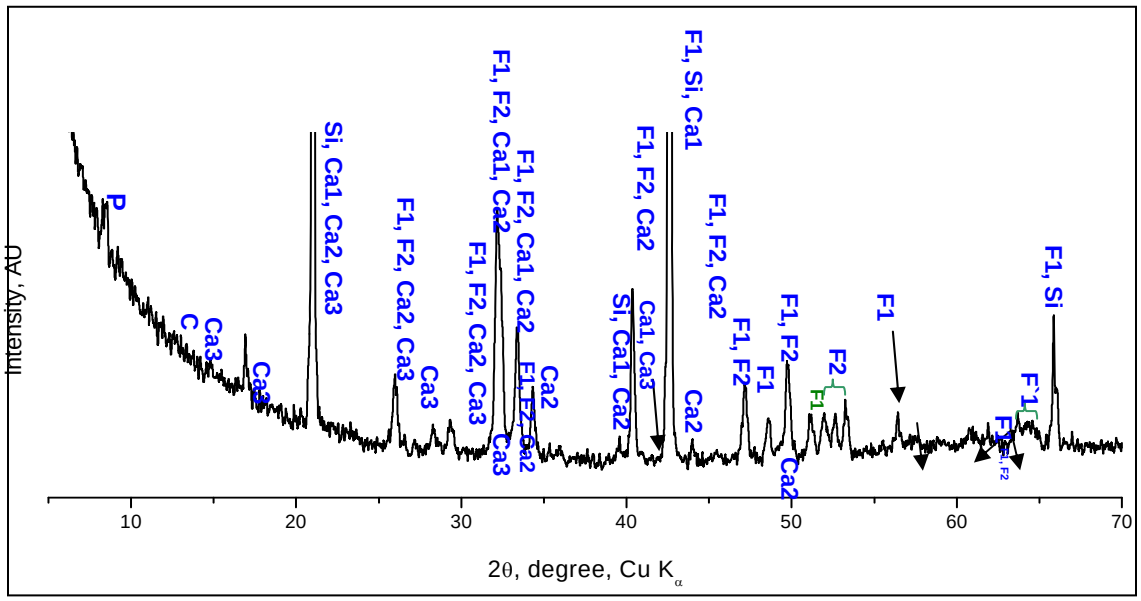

Figure 24. XRD Patterns of Black Particles from Tailings of 1862 Sample.

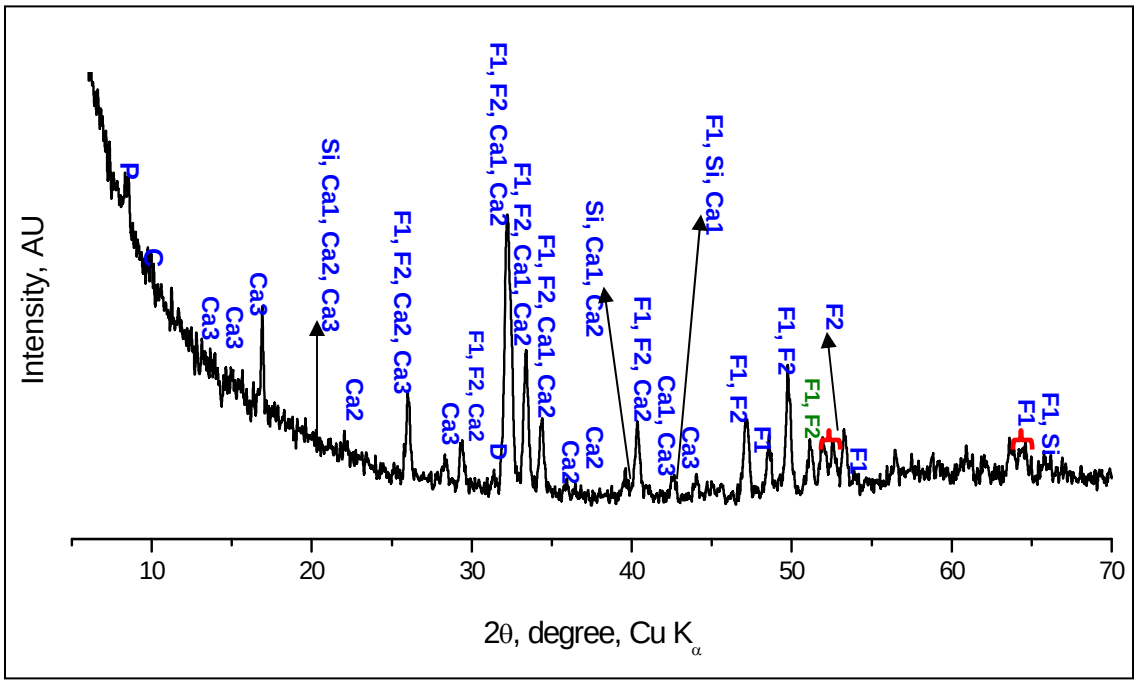

Figure 25. XRD Patterns of Black Particles from Tailings of 3057 Sample.

XRD

XRD analysis performed on *fine* and *coarse* black particles picked up from tailings of FCO Bad as well as fine black particles picked up from tailings of 1862 and 3057 samples (Figures 23 to 25) revealed that all the samples are composed of francolite $CaF(Ca,C)_4[(P,C)(O,OH,F)_4]_3$ and carbonate hydroxyapatite $Ca_{10}(PO_4)_3(CO_3)(OH)_2$ with an admixture of dolomite, and different calcium aluminum silicate hydrates $CaAl_2Si_2O_8{\cdot}4H_2O$ and magnesium aluminum silicates, palygorskite $MgAlSi_4O_{10}(OH) \cdot 4H_2O$ and cordierite $Mg_5(Si,Al)_8O_{20}(OH)_2{\cdot}8H_2O$). Cordierite is a cyclosilicate mineral, a common constituent of contact and regionally metamorphosed argillaceous rocks. Palygorskite (attapulgite) is phyllosilicate clay. The 3057 and FCO Bad samples have a small admixture of dolomite. However, in contrast to the 3057 samples, black particles from tailings of the FCO Bad and 1862 samples have a significant admixture of quartz. White particles picked from tailings of FCO Bad (Figure 23, c) are composed of quartz with a small admixture of the alumosilicates and palygorskite. Francolite $CaF(Ca,C)_4[(P,C)(O,OH,F)_4]_3$ peaks are also observed. This suggests that phosphate is associated with quartz particles or is finely disseminated in quartz (very weak peaks of phosphates/francolite). In that case, the phosphate cannot be liberated for flotation, and hence becomes virtually unrecoverable.

FTIR RESULTS

As seen in Figures 26 to 28, except for the FCO Bad sample, all the ATR spectra measured on coarse particles picked for the analysis from concentrates have a main complex band with a maximum at about 1030 cm^{-1} and a narrow satellite at ~970 cm^{-1}. These features are assigned to the (3P-O stretching vibrations of PO_4 tetrahedra, which confirm that the particles studied are polytypes of apatite. It is known from the literature (Panda and others 2003, Pleshko and others 1991, and Paschalis and others 1996) that both the position and width of the (3P-O band depends on the stoichiometry and crystallinity of apatite (Table 2). In addition, all the spectra have bands at 1456, 1425, and 865 cm^{-1}, typical for carbonate groups, that isomorphically substituted for phosphate groups (Matthews 1977). A strong, broad band at ~840 cm^{-1} is observed in the ATR spectrum of one of the three particles studied from the FCO Bad concentrate sample (Figure 28). This can be assigned to multiphonon infrared absorption of cation-doped periclase (MgO) (Panda and others 2003). Figures 29 to 31 show ATR FTIR spectra of coarse black particles picked up from tailings.

Analysis of the carbonate/phosphate ratio (estimated as a ratio of the integral intensity of the carbonate double band at 1456 and 1425 cm^{-1} to that of the $(PO_4^{3-})_3$ at ~1030 cm^{-1}) in the spectra does not reveal any particular difference between tailings and concentrates in terms of the amount of carbonate substitution (Table 3). In addition, we do not observe a systematic difference between the shift and width of the $(PO_4^{3-})_3$ band of tailings and concentrate. This band is sensitive to the crystallinity of the phosphate (Table 2). Both these observations allow us to conclude that the crystallinity and stoichiometry of apatite/francolite are possibly not the factors that determine the lack of floatability of the phosphate particles studied.

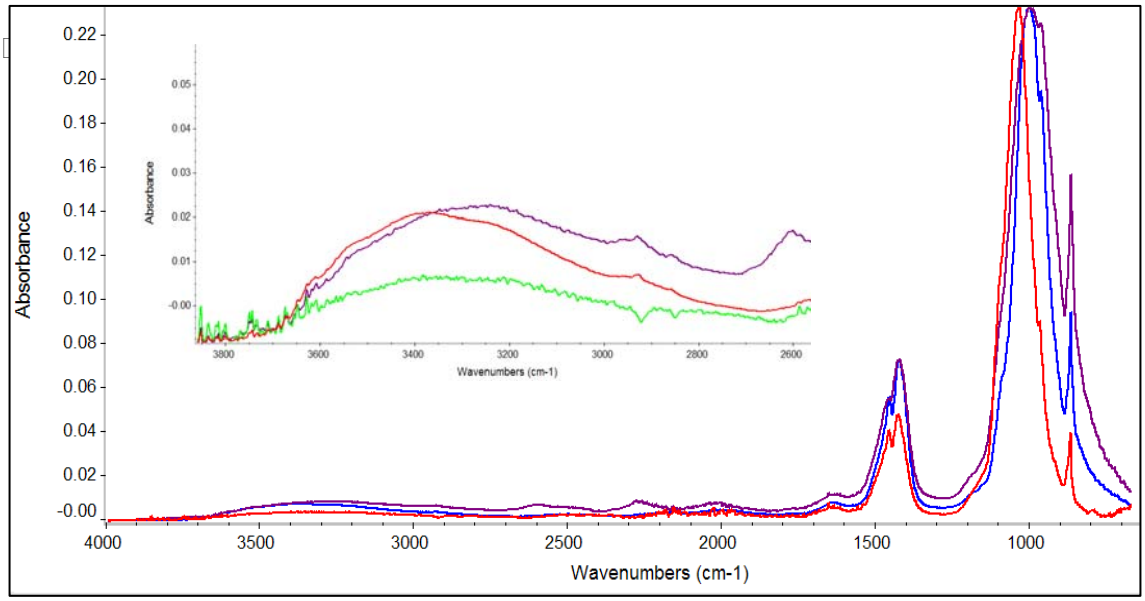

Figure 26. ATR Spectra of Three Coarse Black Particles Picked from the Concentrate of CF East Sample. Insert shows enlarged region due to stretching vibrations of the OH groups.

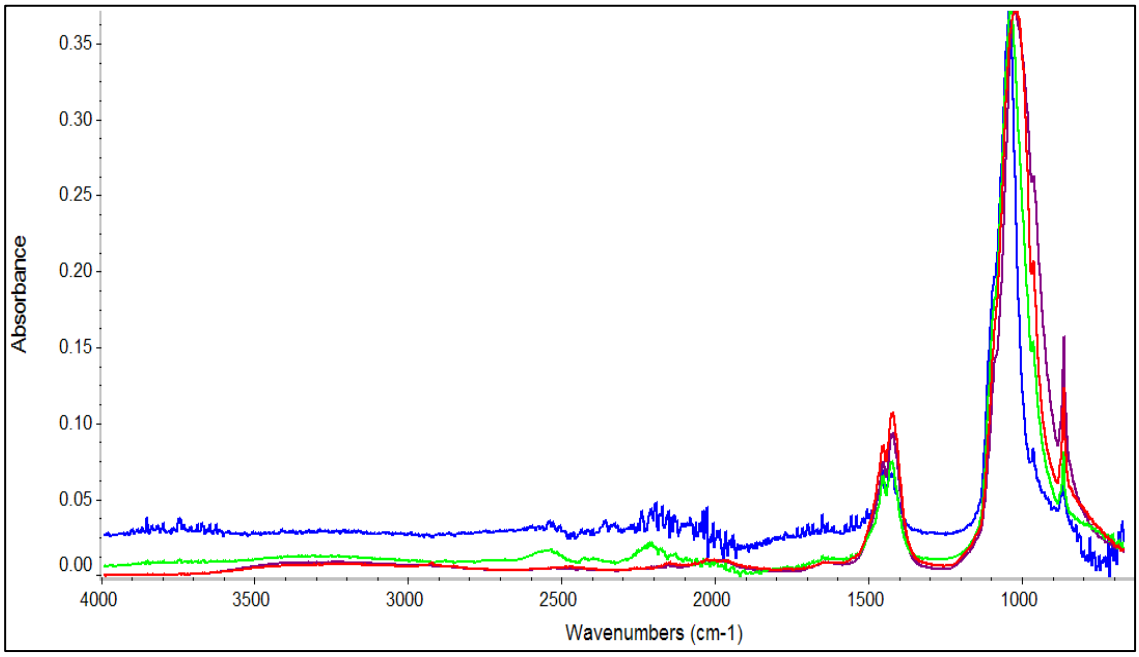

Figure 27. ATR Spectra of Four Coarse Black Particles Picked from the Concentrate of 3057-S2 Sample.

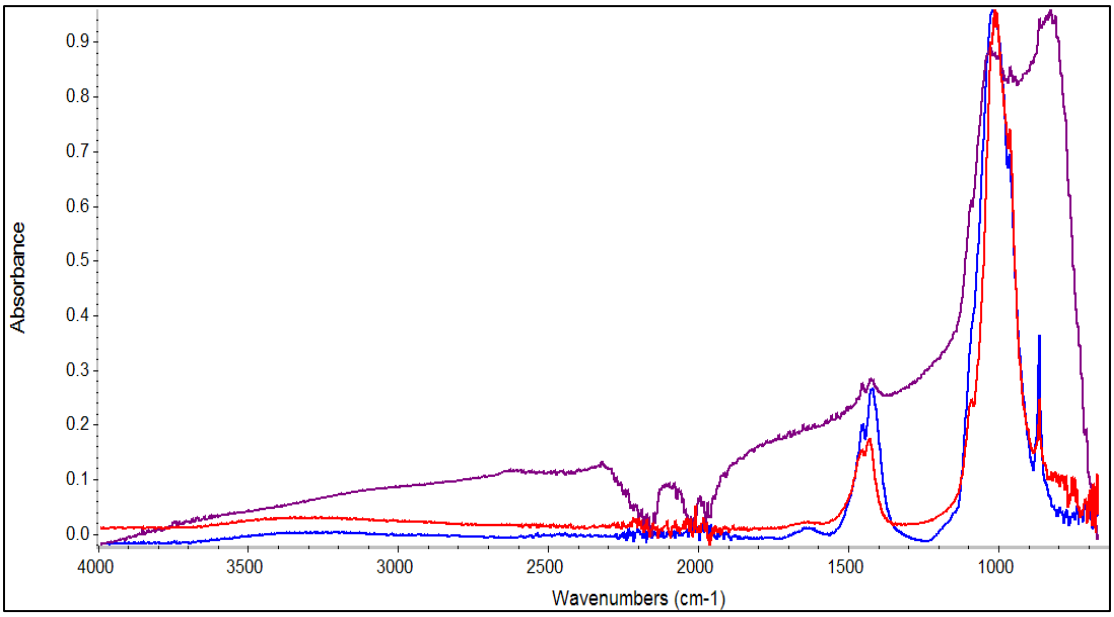

Figure 28. ATR Spectra of Three Coarse Black Particles Picked from the Concentrate of FCO Bad Sample.

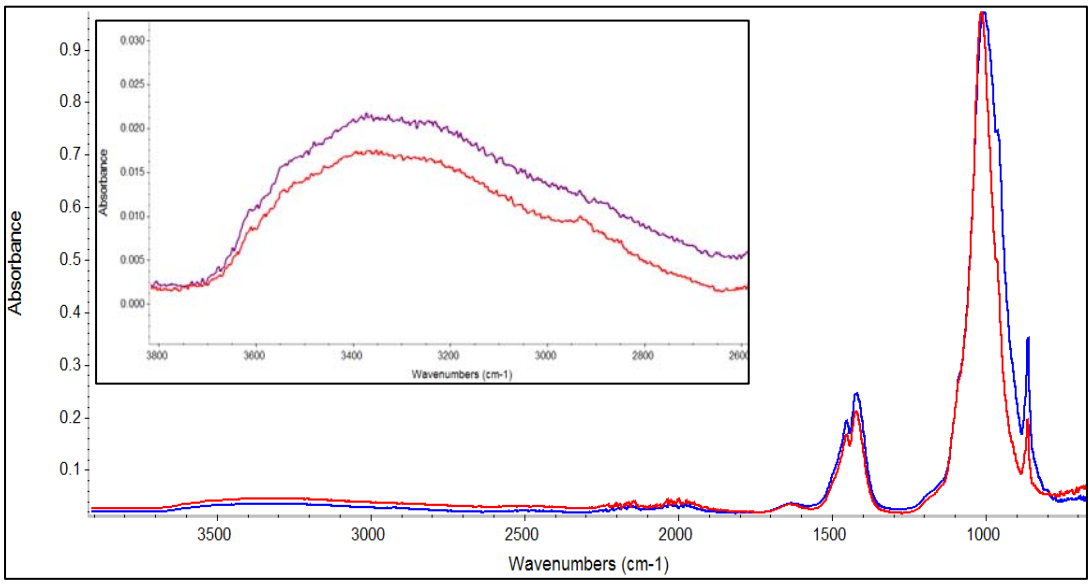

Figure 29. ATR Spectra of Two Coarse Black Particles Picked from Tailings of CF East Sample. Insert shows enlarged region due to OH groups.

Table 2. Major Components of the PO_4^{3-} Band (Pleshko and others 1991).

Band Position, cm^{-1}	Assignment
960	$\nu_1 PO_4^{3-}$
996	PO_4^{3-} in apatitic environment
1020	Persistence of vacancies; nonstoichiometric apatites containing HPO_4^{2-} and/or CO_3
1032	PO_4^{3-} in stoichiometric apatites
1034	Type B carbonate apatites; hydroxyapatite
1056	Bands corresponding to the T_2 vibrational modes of apatite
1075	Bands corresponding to the T_2 vibrational modes of apatite
1092	Stoichiometric apatites
1109	Poorly crystalline apatites
1123	HPO_4^{2-}
1143	Apatites containing HPO_4^{2-}

A more detailed comparison of non-phosphate bands in the ATR spectra shows differences between tailings and concentrates that are specific for each sample. In particular, as can be seen from the comparisons of tailings and concentrate of CF East sample (Figures 26 and 29), tailings are characterized by the higher intensity of a band at about 3620 cm^{-1}. This band originates from the stretching vibrations of the acidic bridged hydroxyls associated with tetrahedrally coordinated framework aluminum atoms (Al T-atoms) (Pleshko and others 1991). This Al-OH-A1 band at about 3620 cm^{-1} is common for the spectra of all Al-containing silicates (Pleshko and others 1991). Figures 32 and 33 show this band in the IR spectra of muscovite and kaolinite, respectively. The higher presence of alumosilicate inclusions in tailings compared to the concentrate of CF East sample is more evident from the comparison of the transmission spectra measured on particles from concentrate and tailings of the CF East sample (Figures 34 and 35, respectively). The alumosilicate/phyllosilicate impurity (muscovite or highly-defective kaolinite) is characterized by the distinct Al-OH-A1 band due to acidic hydroxyls at 3620 cm^{-1}, along with a pair of bands at 800 and 780 cm^{-1} due to stretching vibrations of SiO_4 tetrahedra, typical for quartz and alumosilicates (Paschalis and others 1996). The associated bending vibration of the Al–OH–Al groups is observed as a shoulder at about 915 cm^{-1} (Figure 34).

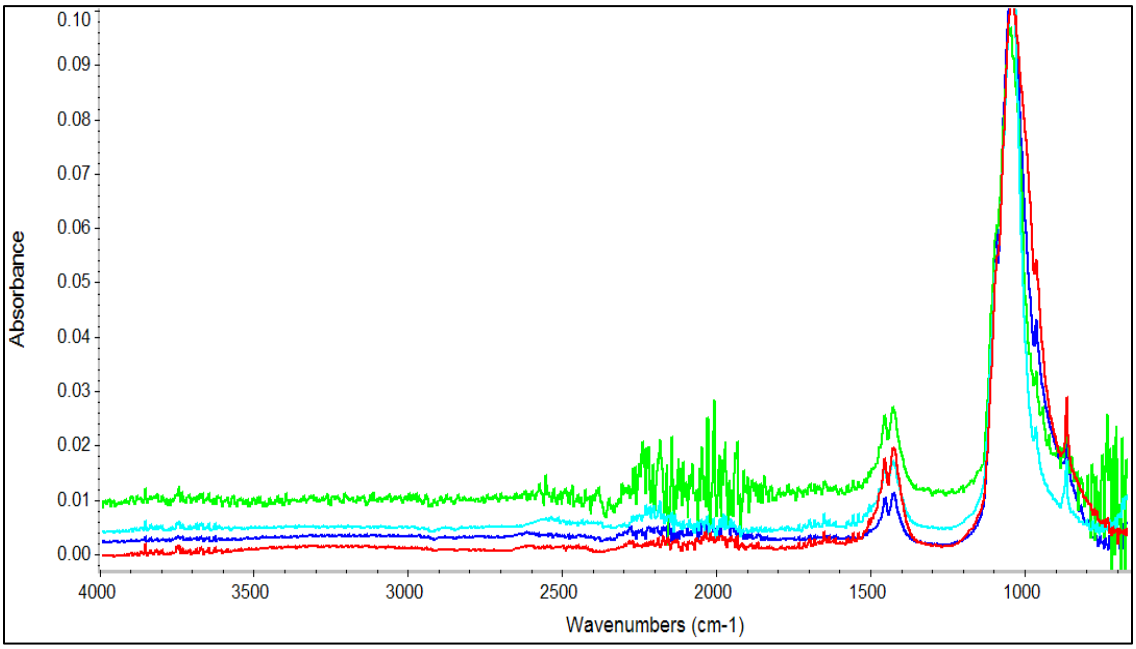

Figure 30. ATR Spectra of Four Coarse Black Particles Picked from Tailings of 3057-S2 Sample.

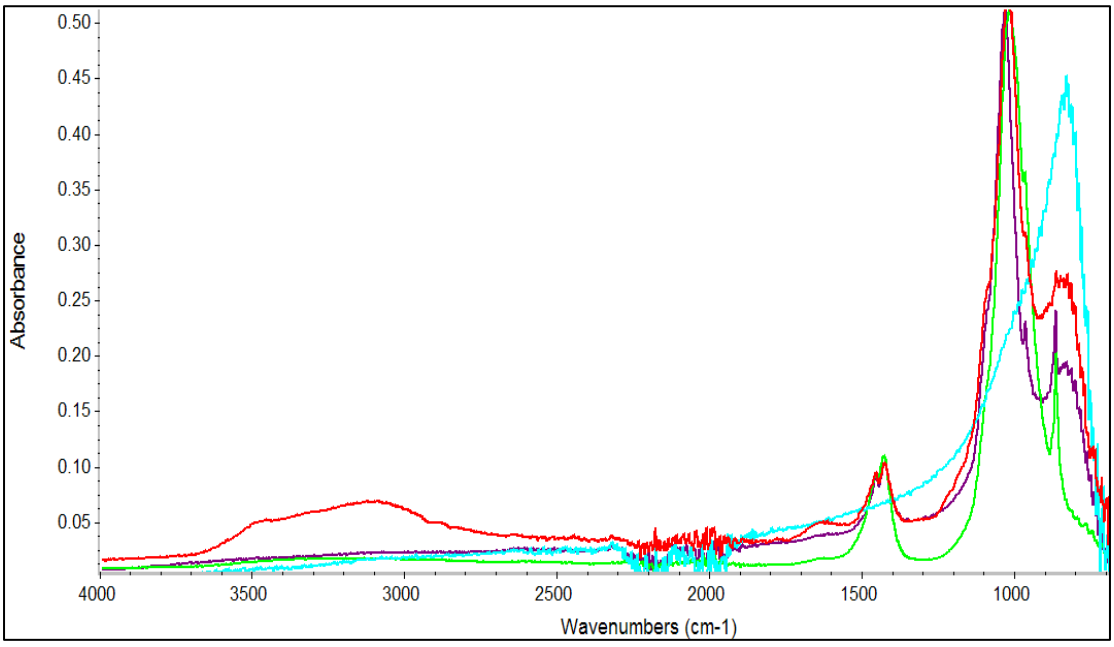

Figure 31. ATR Spectra of Four Coarse Black Particles Picked from Tailings of FCO Bad Sample.

Table 3. Ratio Between Carbonate (1425 cm^{-1}, 1456 cm^{-1}) and Phosphate (1030 cm^{-1}) Peaks Calculated Using ATR Spectra of Three Different Samples for Both Concentrate and Tailings.

Ore Sample	Particle Number	Carbonate/Phosphate Peak Area
FCO Bad (Conc)	1	0.44
	2	0.01
	3	0.15
FCO Bad (Tails)	1	0.13
	2	0.12
	3	0.11
3057-S2 (Conc)	1	0.11
	2	0.13
	3	0.16
3057-S2 (Tails)	1	0.13
	2	0.05
	3	0.11
	4	0.11
CF East (Conc)	1	0.14
	2	0.14
	3	0.17
CF East (Tails)	1	0.16
	2	0.15

Figure 36 shows transmission and reflection spectra of a fine brown particle picked from tailings of the 1862 sample. It follows from a comparison of these spectra that although this particle is mostly francolite in the bulk, its surface is enriched by silanol groups (a narrow band at 3745 cm^{-1}) and an oxide (a broad band at 840 cm^{-1}). The latter is tentatively assigned to periclase (MgO). However, a more definite conclusion can be done based on the XRD analysis. Since bands at 780 and 800 cm^{-1} of stretching vibrations of SiO_4 tetrahedra are not observed in the spectra, it can be concluded that the silanols are not due to silicate/alumosilicate bulk inclusions. The difference between the surface and the bulk is more pronounced for a coarse black particle from the 1862 sample. As seen in Figure 37, periclase dominates on its surface, while francolite dominates in the bulk.

Based on these data, it can be concluded that mineralogical composition of the surface and the bulk are different for both fine and coarse particles of 1862. In addition, the surface of a fine particle has silanol groups.

With respect to the spectra of the CF East concentrate (Figure 34), the OH bending band of water at about 1630 cm^{-1} from tailings is narrow and split into two components. This suggests the presence of intercalated water in sheet-structured alumosilicate impurities of tailings. In addition, one particle from the CF East tailings

(the red line in Figure 35) is characterized by a band at 3745 cm^{-1}, which is characteristic of surface silanol groups.

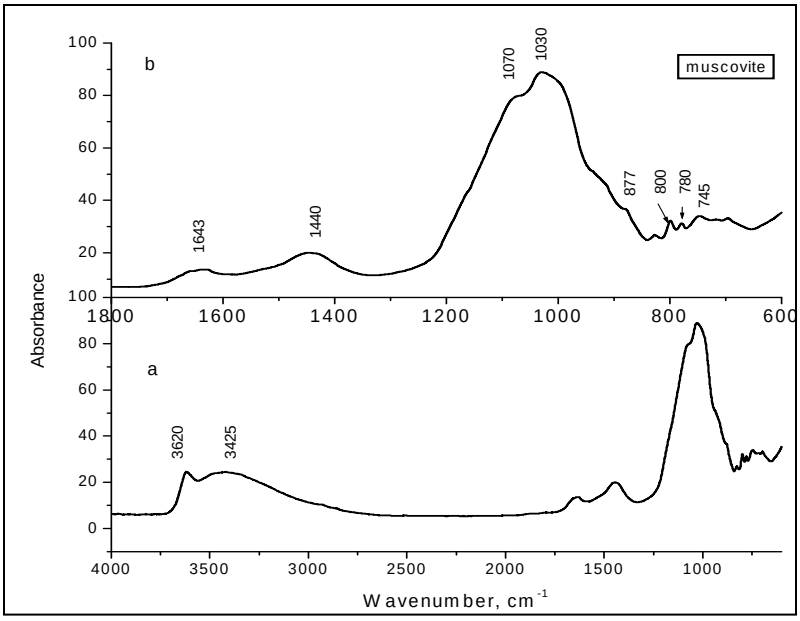

Figure 32. Transmission IR Spectrum of Muscovite (Spectral Library of Johns Hopkins University).

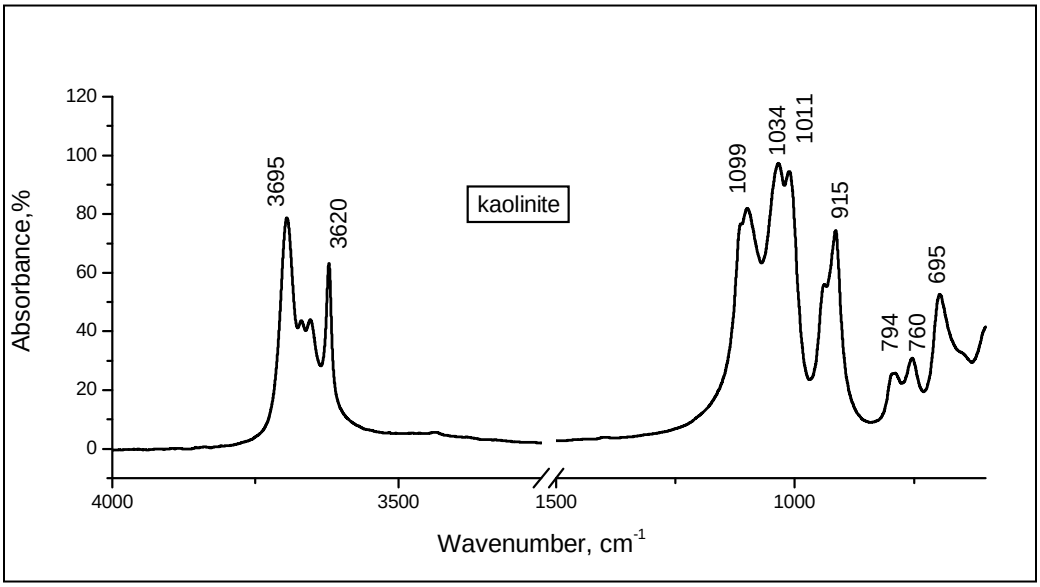

Figure 33. Transmission IR Spectrum of Well-Crystallized Kaolinite (Spectral Library of Johns Hopkins University).

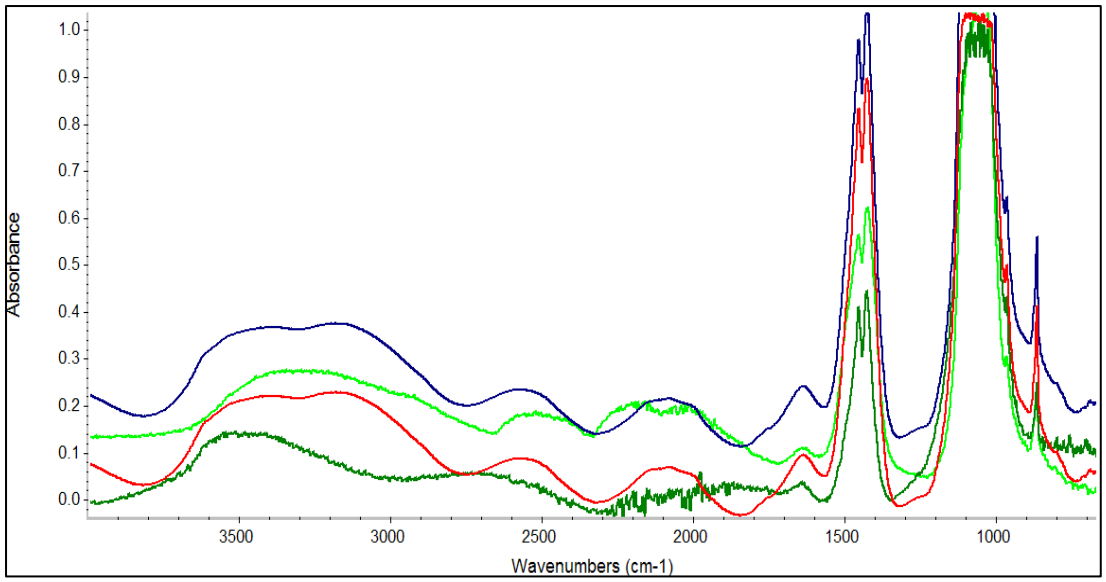

Figure 34. FTIR Transmission Spectra of Four Coarse Black Particles Picked from Concentrate of CF East Sample.

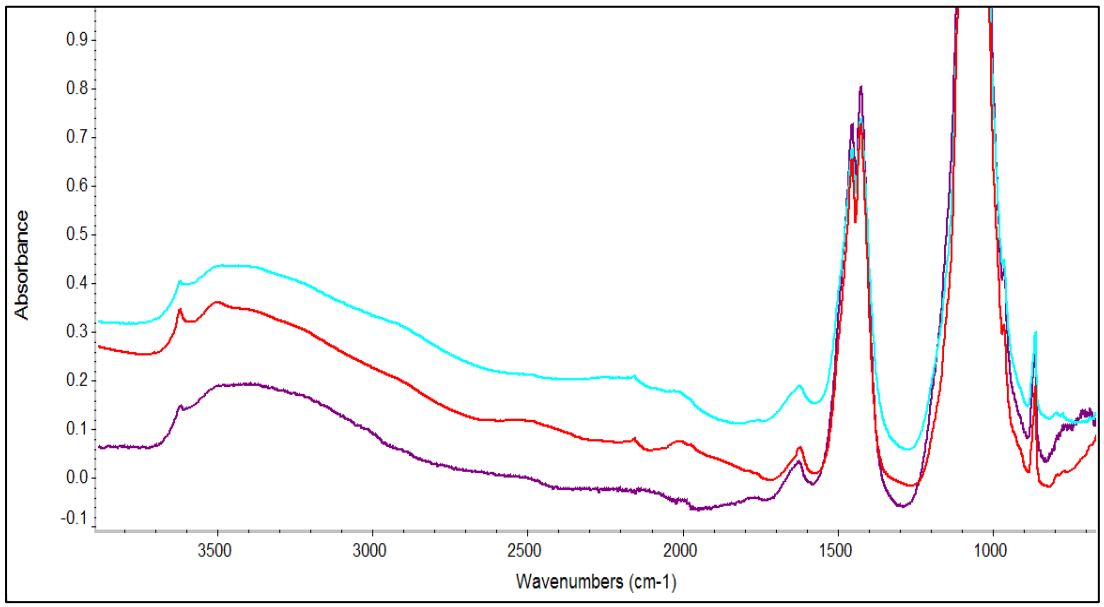

Figure 35. ATR Spectra of Three Coarse Black Particles Picked from Tailings of CF East Sample.

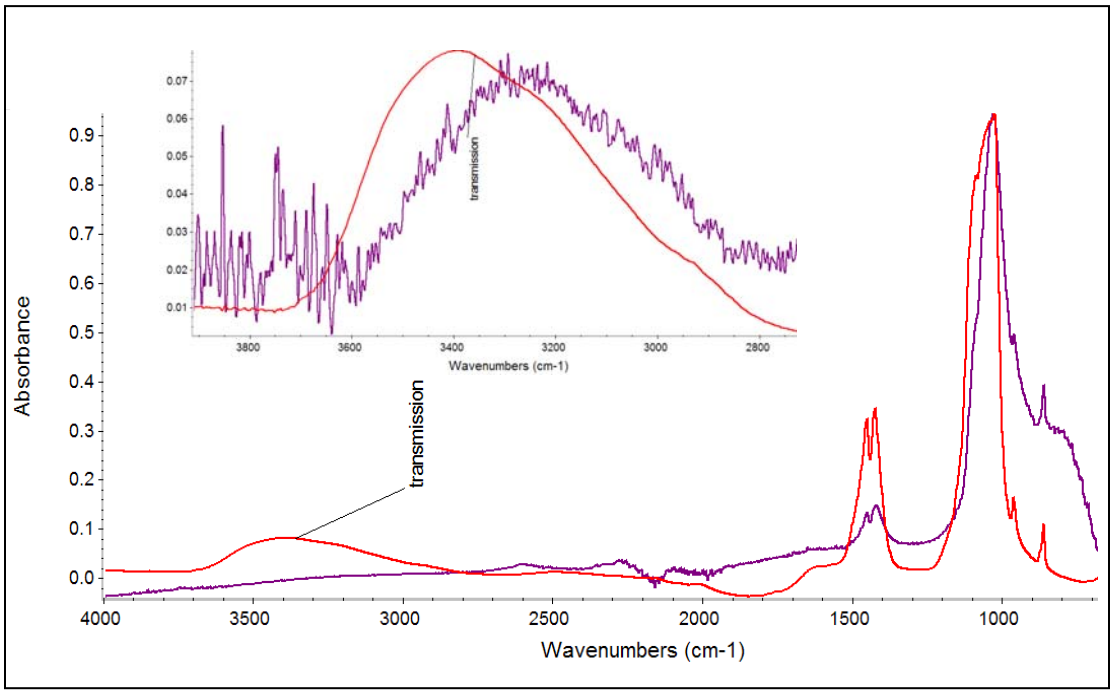

Figure 36. FTIR Transmission (Red) and Reflection (Violet) Spectra of a Fine Brown Particle Picked from Tailings of 1862 Sample. Insert shows enlarged region due to OH groups.

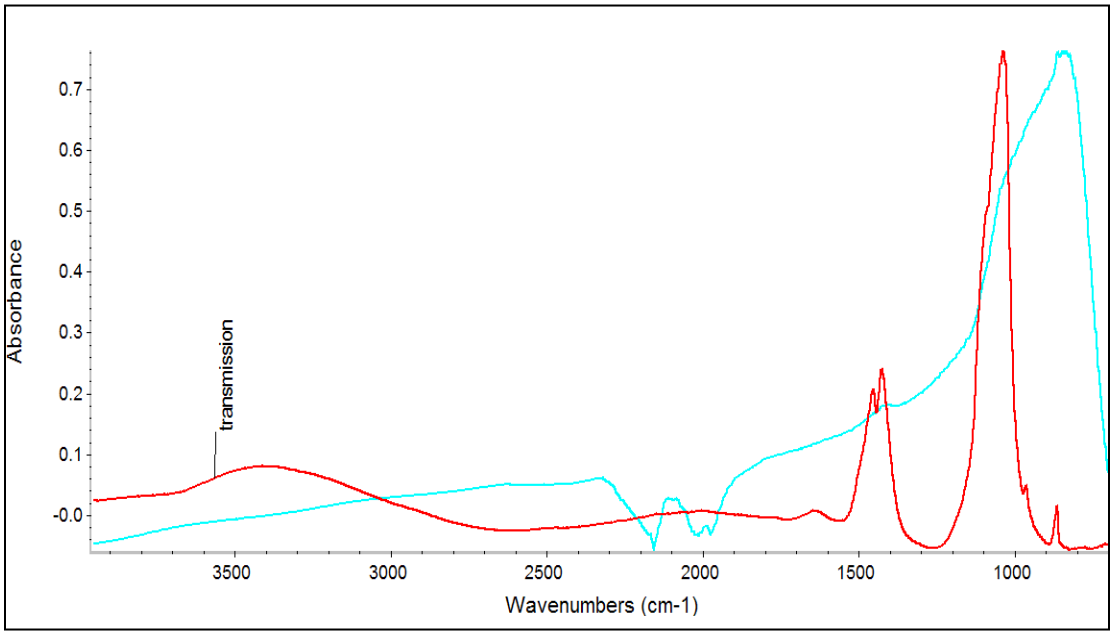

Figure 37. FTIR Transmission (Red) and Reflection (Cyan) Spectra of a Coarse Black Particle Picked from Tailings of 1862 Sample.

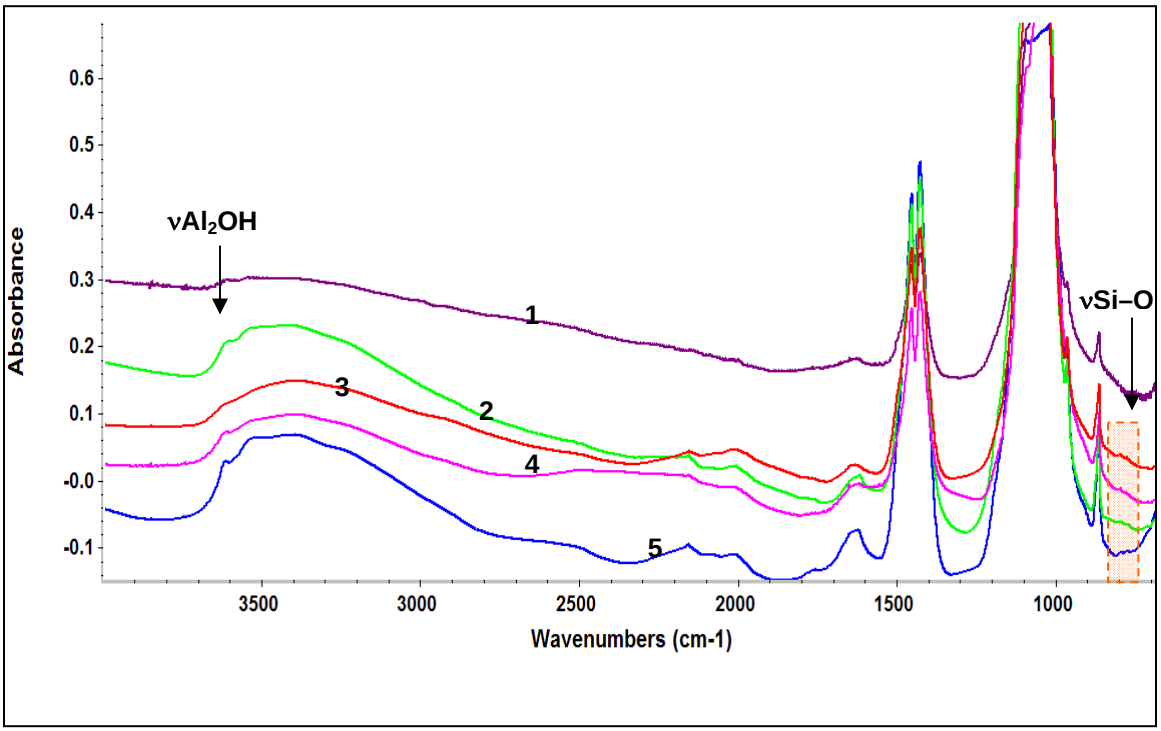

Figure 38. FTIR Transmission Spectra of Fine Black Particles Picked from Tailings of FCO Bad Sample.

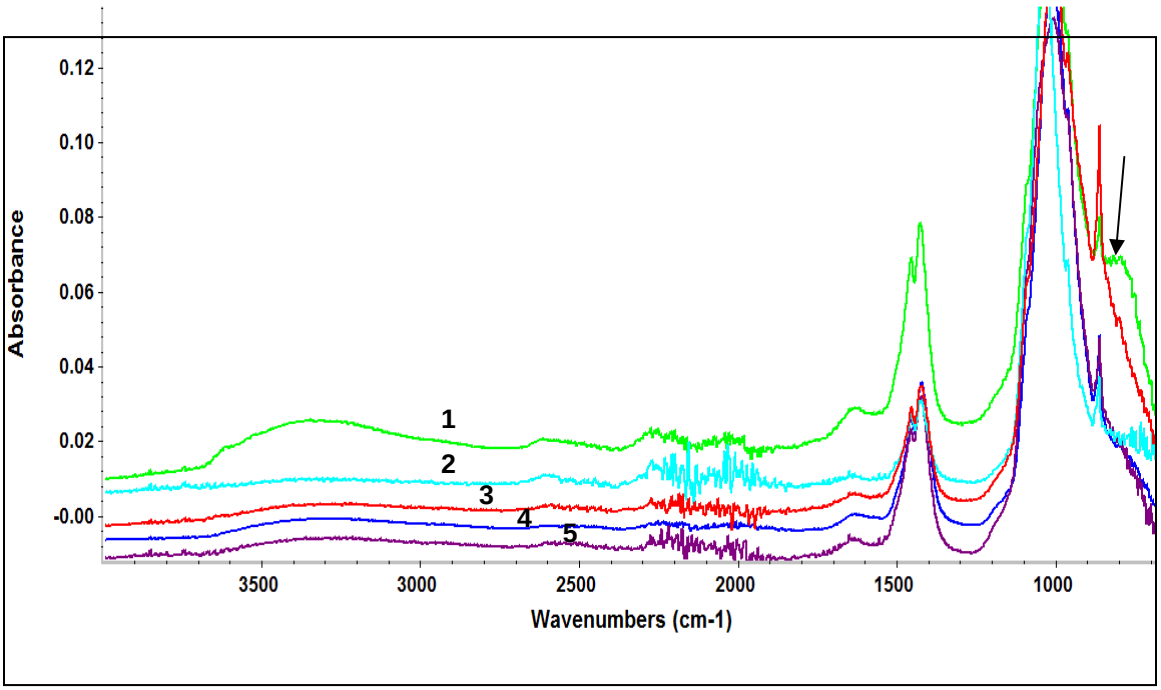

Figure 39. FTIR ATR Spectra of the Same Fine Black Particles Picked from Tailings of FCO Bad Sample as in Figure 44. Arrow shows an artifact band (see text).

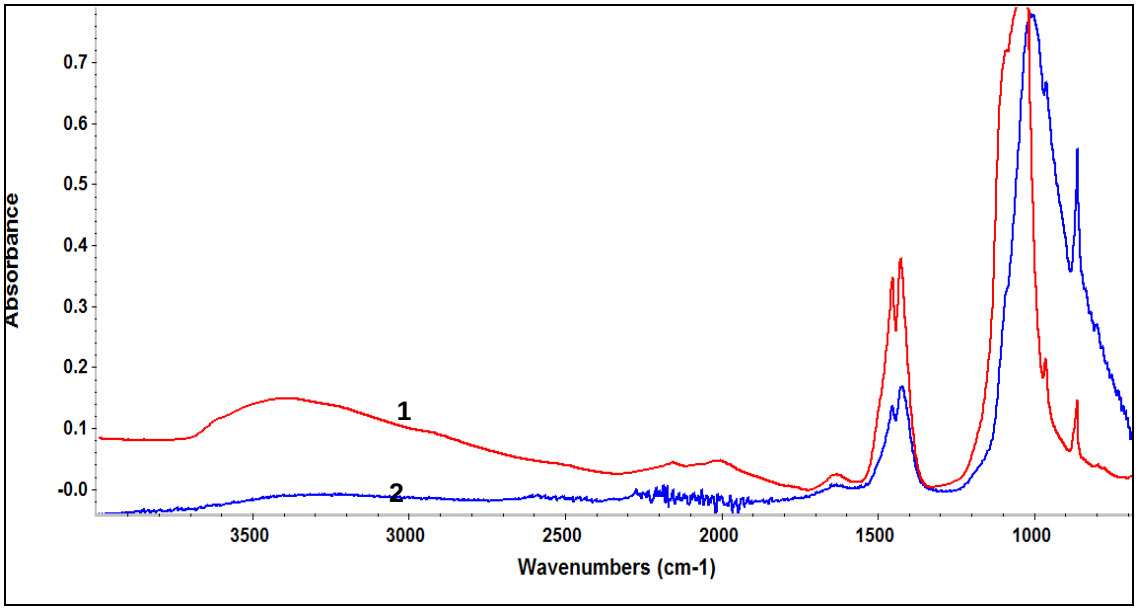

Figure 40. Comparison of FTIR Transmission (1) and ATR (2) Spectra Measured on the Same Fine Black Particle Picked from Tailings of FCO Bad Sample.

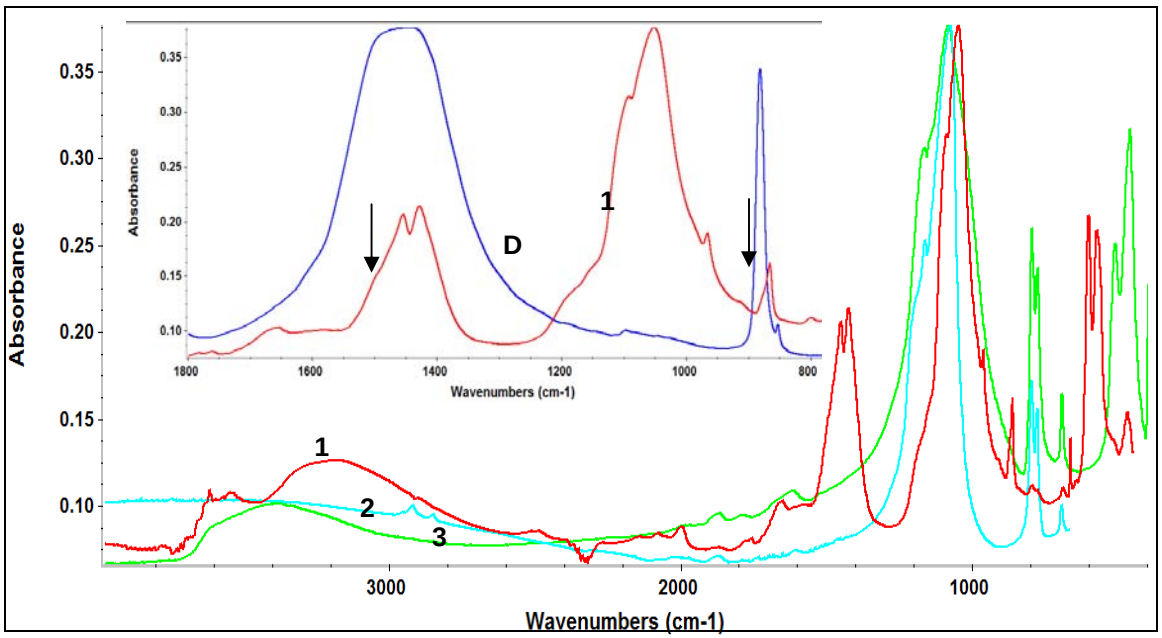

Figure 41. Comparison of FTIR Spectra of (1) Fine Black Particle Picked from Tailings of FCO Bad Sample Measured by Diffuse Reflectance; (2) Fine Particle Number 4 Picked from Tailings of 3057 Sample Measured by Transmission (Figure 30); (3) Quartz from Johns Hopkins University Spectral Library Measured by Transmission. Insert shows contribution of dolomite into FCO Bad spectrum. D = dolomite from Johns Hopkins University Spectral Library measured by transmission.

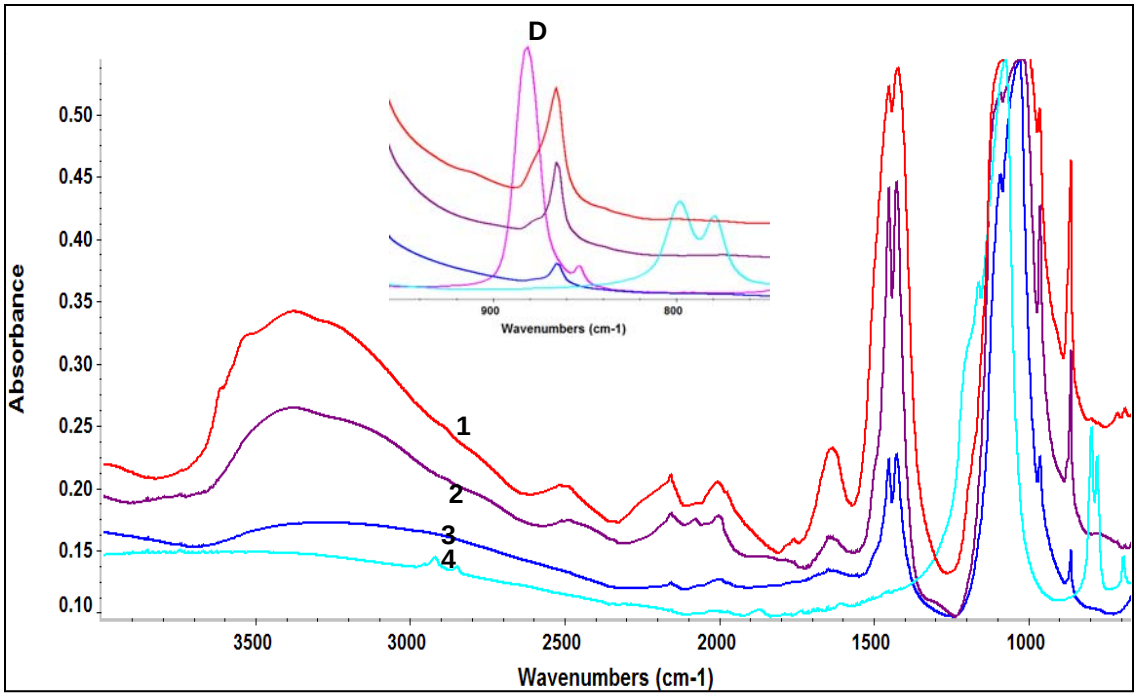

Figure 42. FTIR Transmission Spectra of Fine Black Particles Picked from Tailings of 3057 Sample. Insert shows the δCO_3 vibration, where D marks transmission spectrum of dolomite.

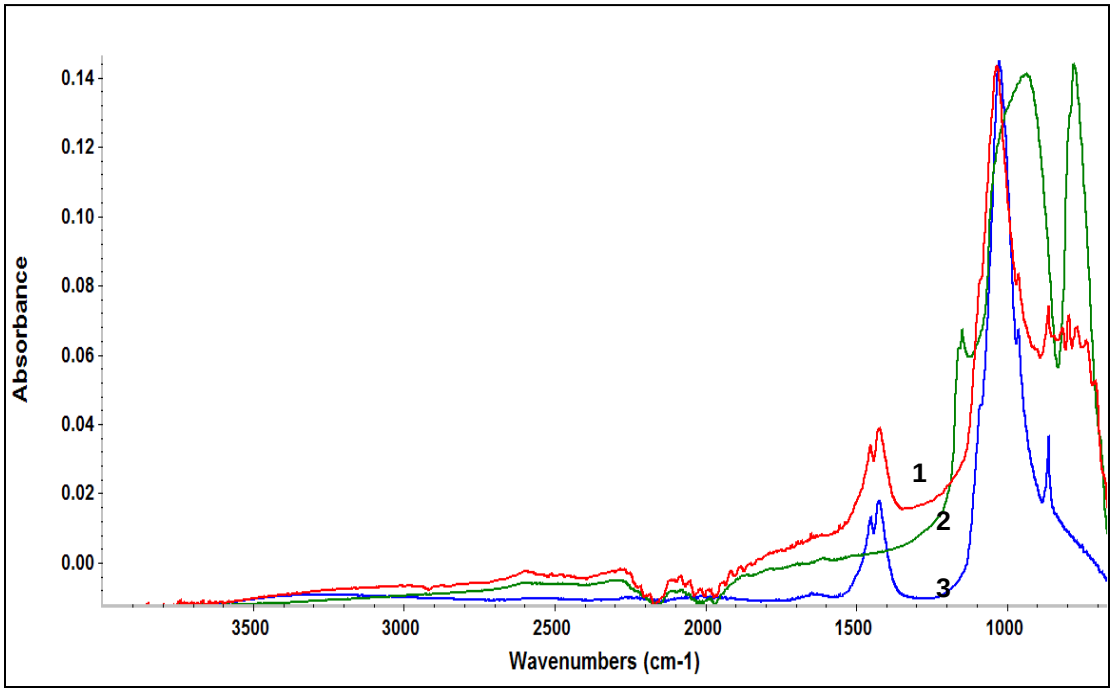

Figure 43. FTIR ATR Spectra of Fine Black Particles Picked from Tailings of 3057 Sample: 1 – Coarse; 2, 3 – Fine.

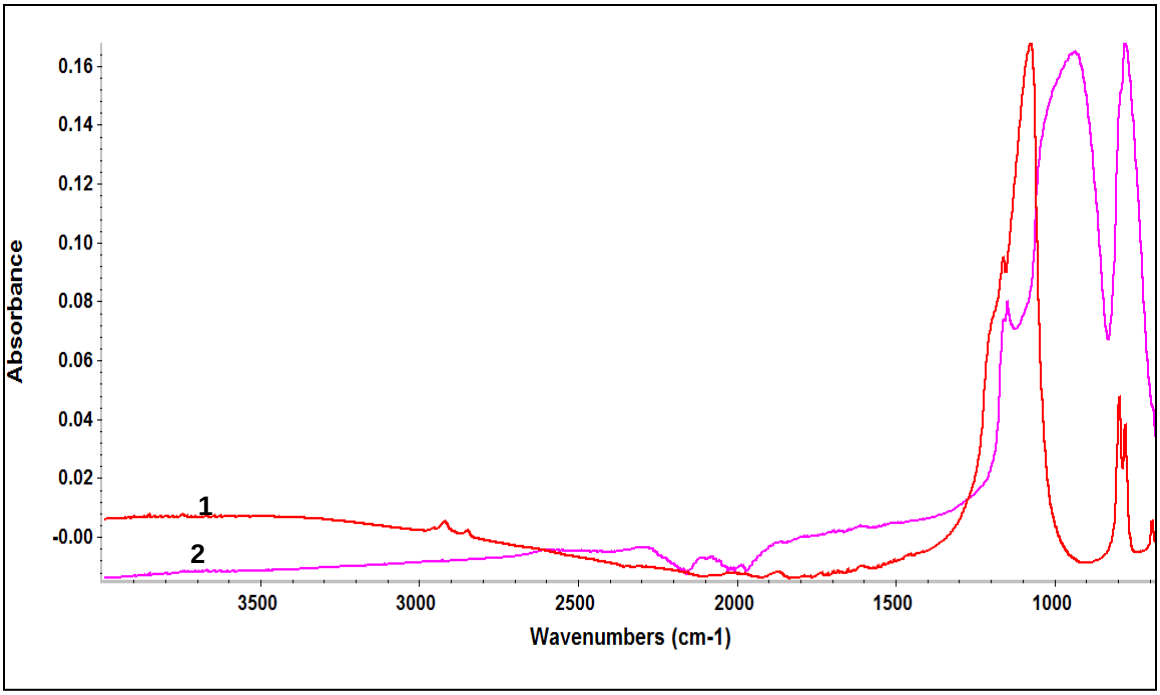

Figure 44. Comparison of FTIR Transmission (1) and ATR (2) Spectra Measured on the Same Fine Black Particle Picked from Tailings of 3057 Sample.

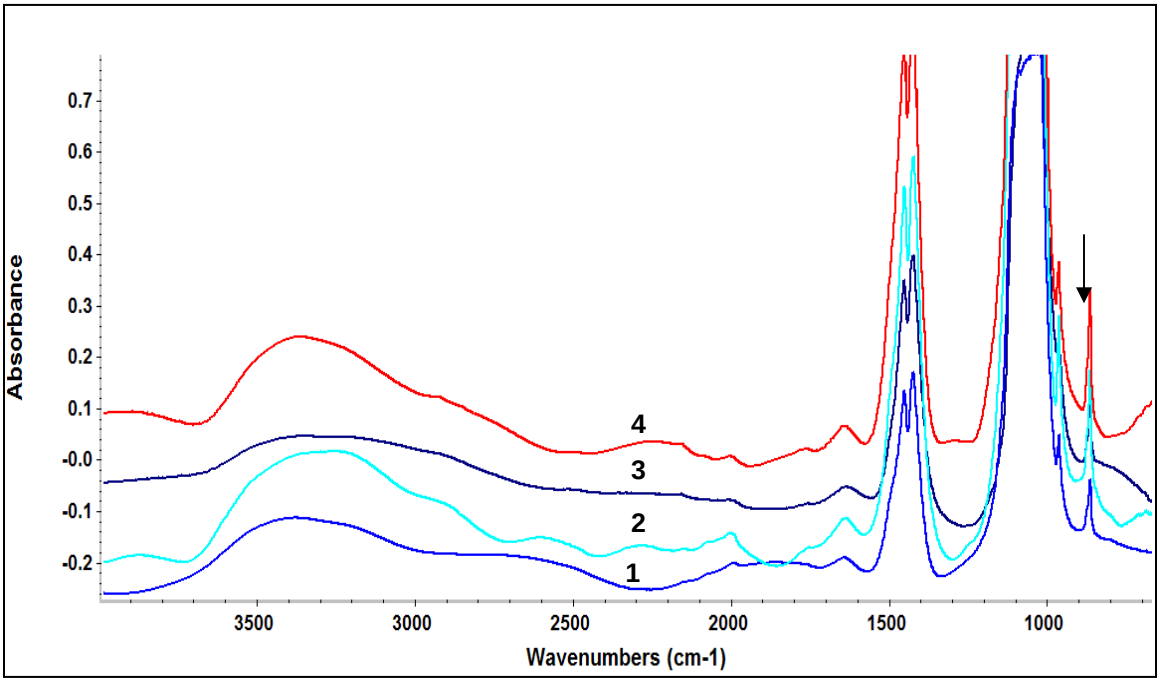

Figure 45. FTIR Transmission Spectra of Fine Black Particles Picked from Concentrate of CF West Sample. Arrow marks dolomite.

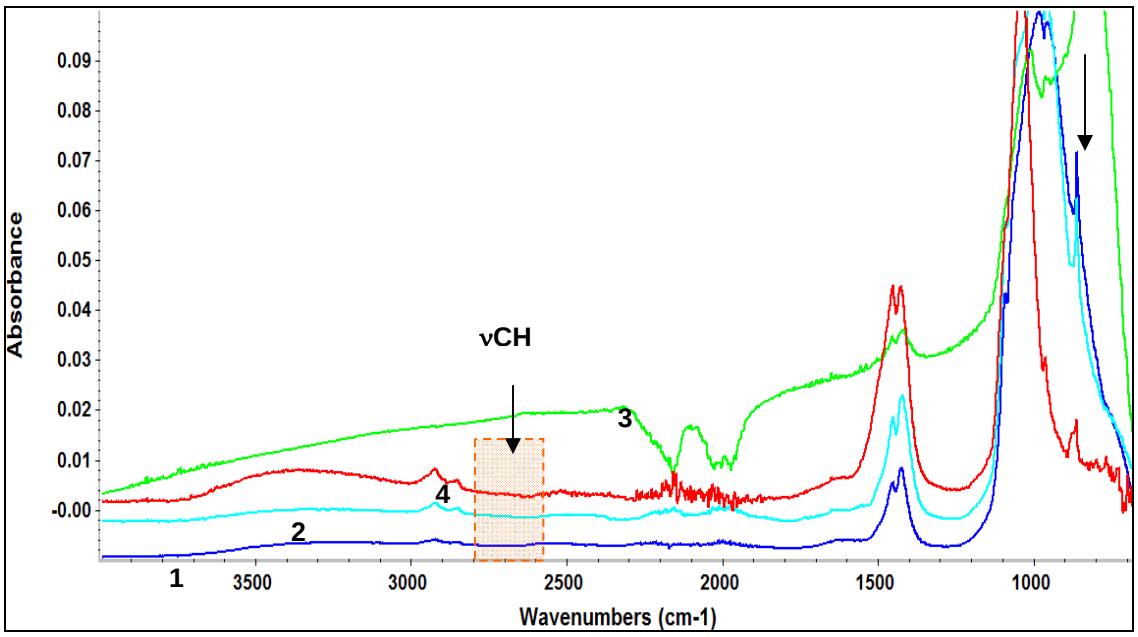

Figure 46. FTIR ATR Spectra of the Same Fine Black Particles Picked from Concentrate of CF West Sample as in Figure 39. Arrow marks dolomite.

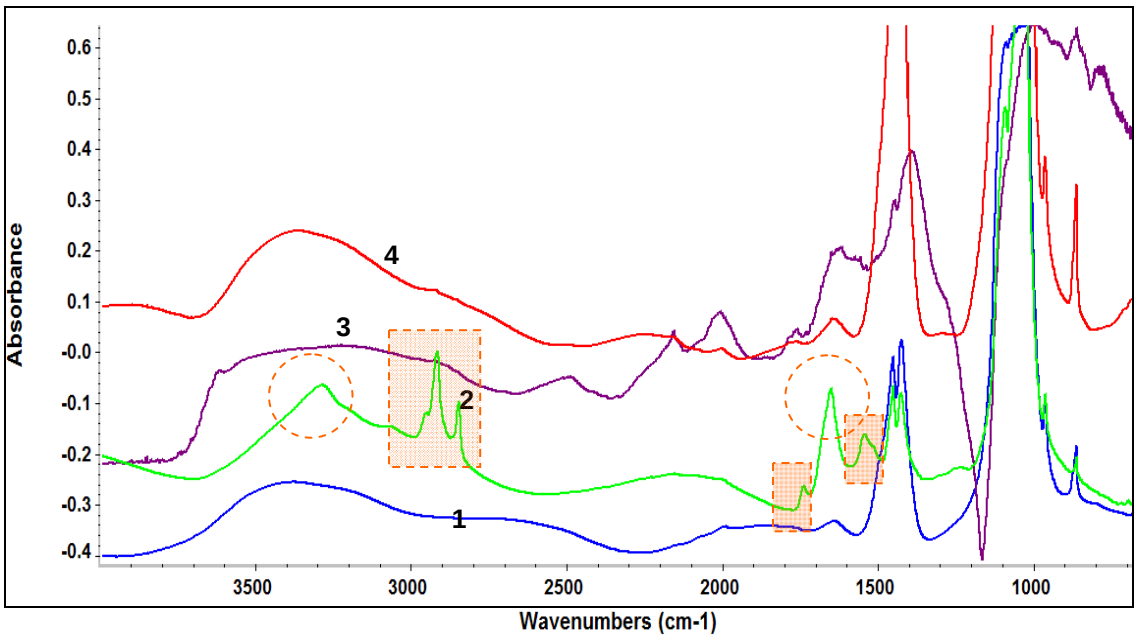

Figure 47. FTIR Transmission Spectra of Fine Black Particles Picked from Tailings of CF West Sample. Boxes mark absorption bands due to CH groups at ~2900 cm^{-1} as well as molecular and deprotonated and carboxylic groups of organic matter at 1740 cm^{-1} (νC=O) and 1550 cm^{-1} ($\nu_{as}OCO^{-}$), respectively. Circles mark stretching (νNH) and bending (δNH) vibrations of molecular amine groups at 3290 and 1660 cm^{-1}, respectively.

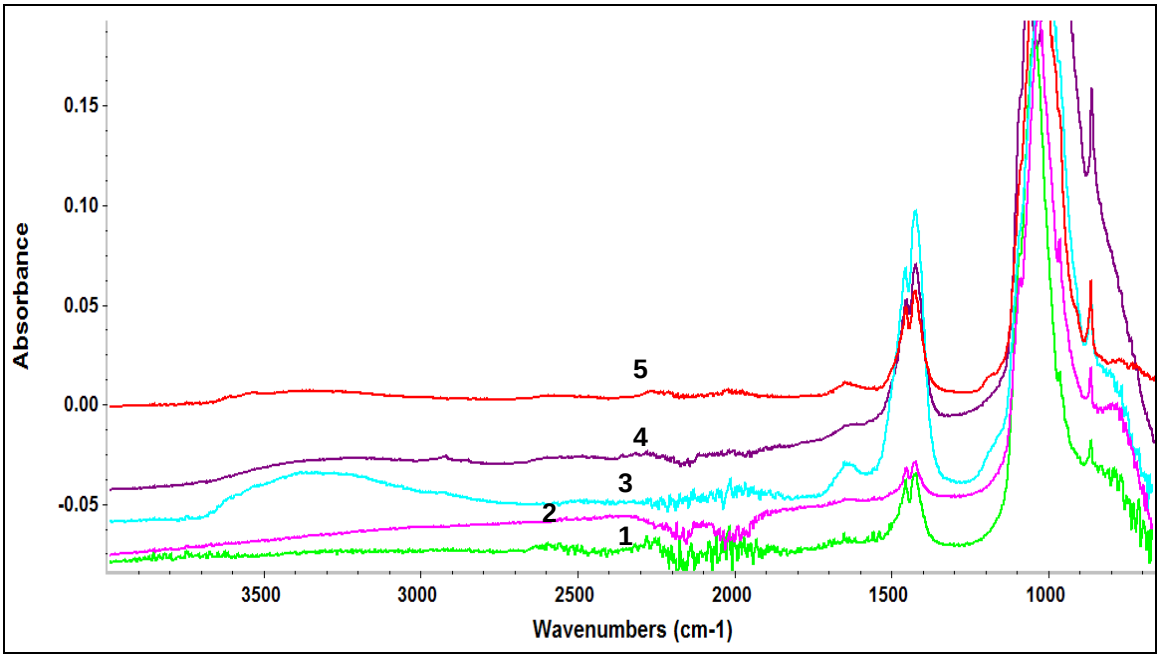

Figure 48. FTIR ATR Spectra of Fine Black Particles Picked from Tailings of CF West Sample.

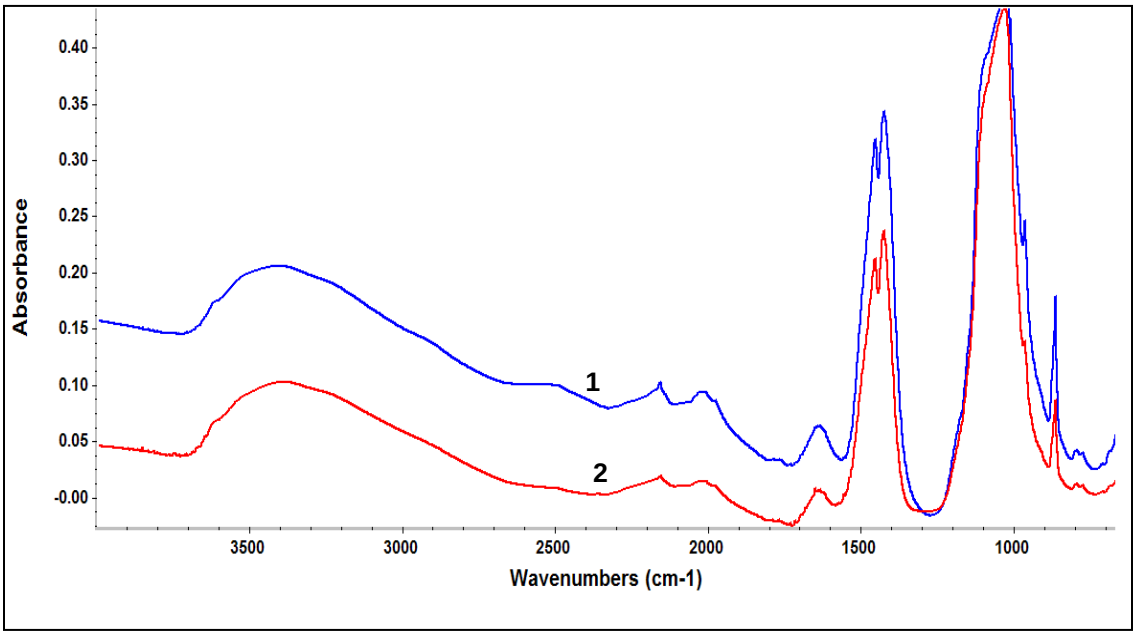

Figure 49. FTIR Transmission Spectra of Fine Black Particles Picked from Tailings of CF East Sample.

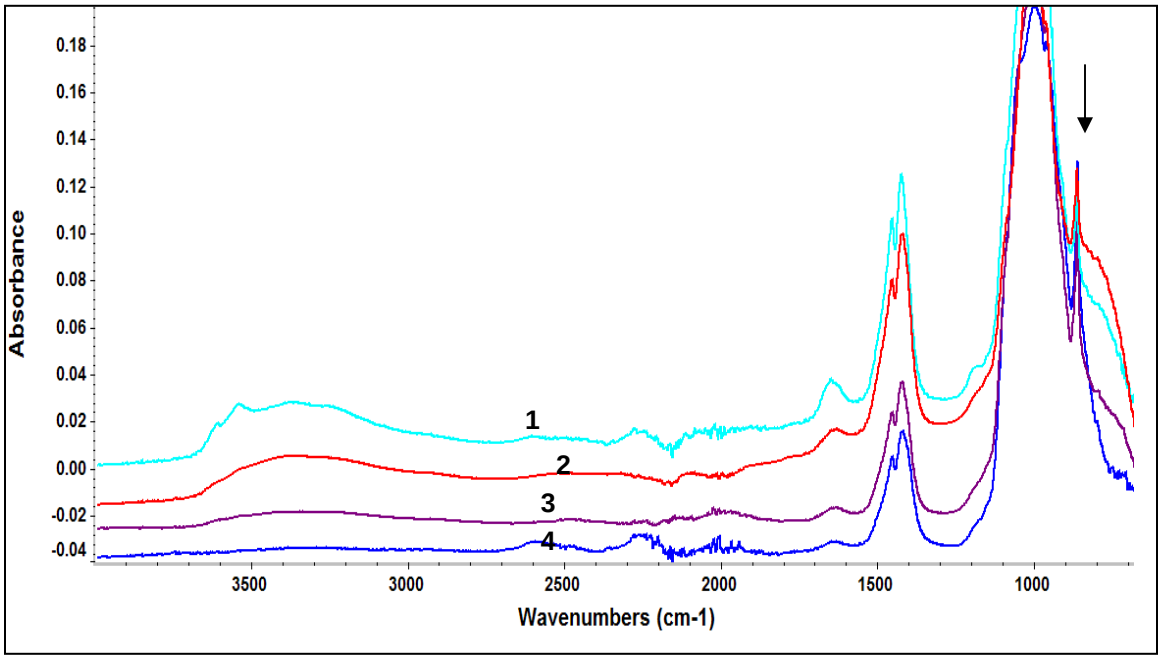

Figure 50. FTIR ATR Spectra of Black Particles Picked from Tailings of CF East 1, 2, 4 – Fine, 3 – Coarse. Arrow shows artifact band.

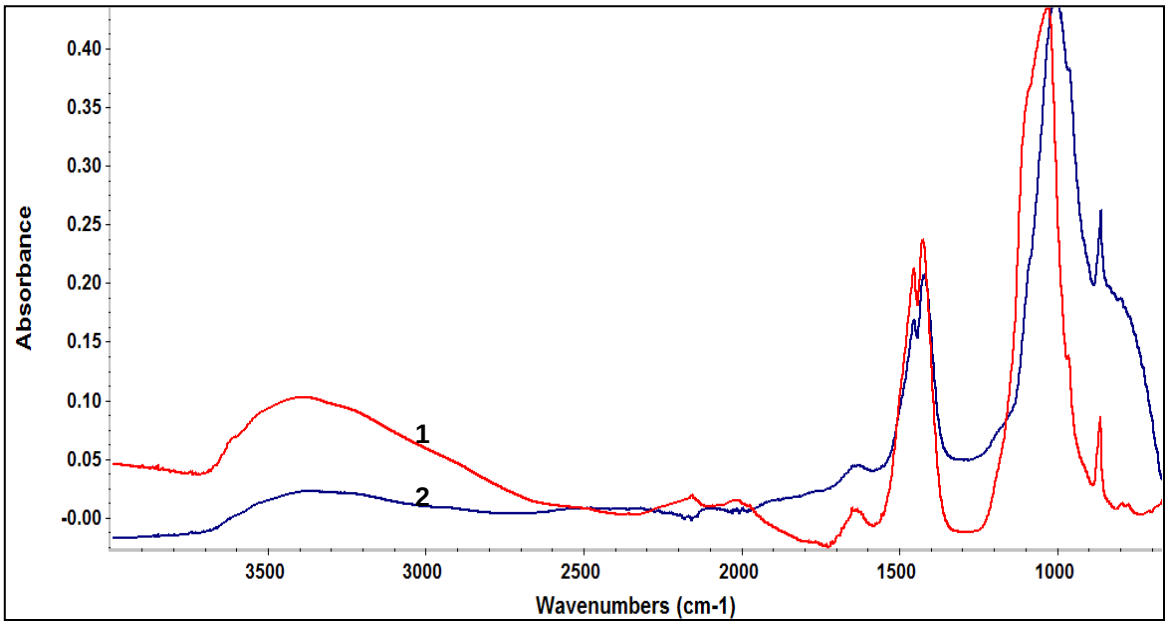

Figure 51. Comparison of FTIR Transmission (1) and ATR (2) Spectra Measured on the Same Fine Black Particle Picked from Tailings of CF East Sample.

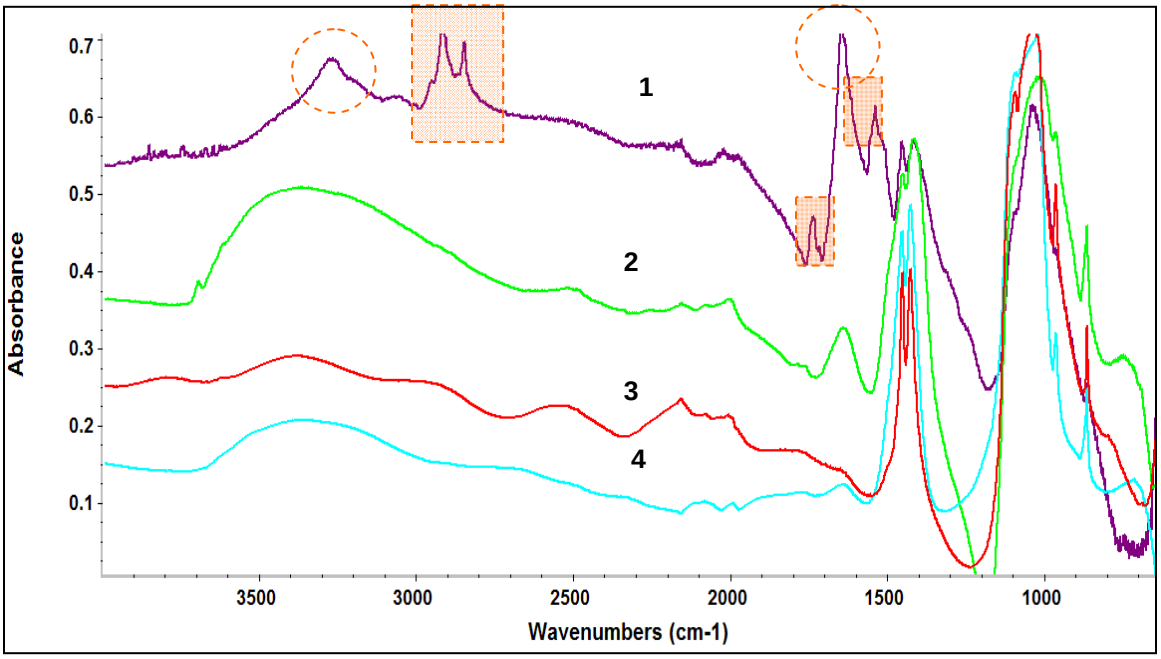

Figure 52. FTIR Transmission Spectra of Fine Black Particles Picked from Tailings of 464-S2. Boxes mark absorption bands due to CH groups at ~2900 cm^{-1} as well as molecular and deprotonated and carboxylic group of organic matter at 1740 cm^{-1} (νC=O) and 1550 cm^{-1} ($\nu_{as}OCO^{-}$), respectively. Circles mark stretching (νNH) and bending (δNH) vibrations of molecular amine groups at 3290 and 1660 cm^{-1}, respectively.

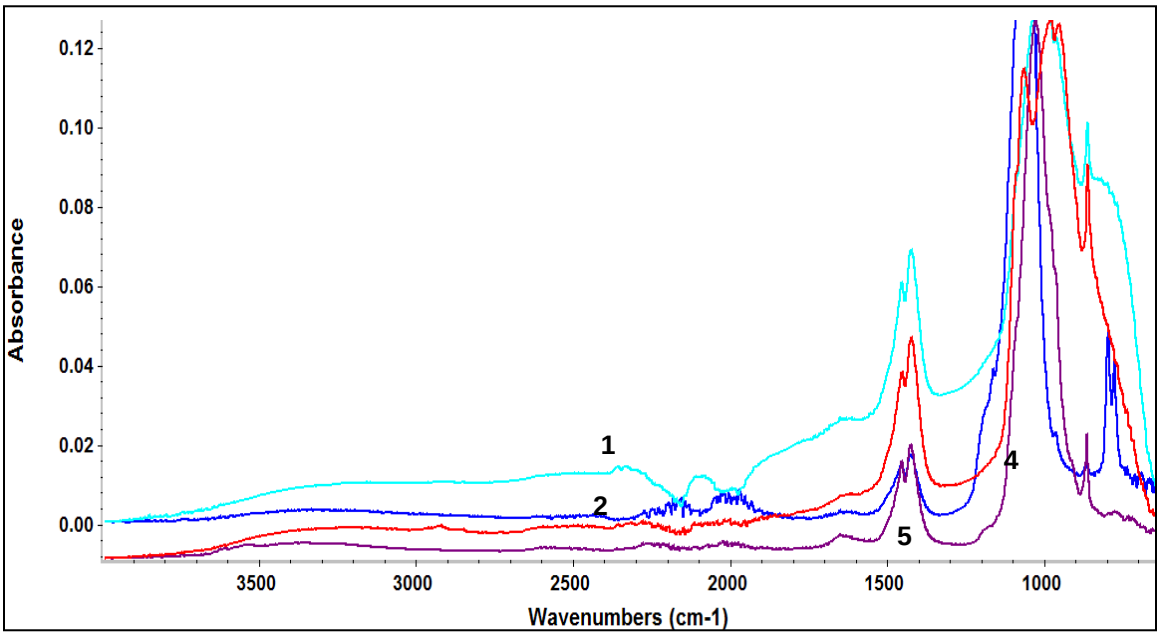

Figure 53. FTIR ATR Spectra of Fine Black Particles Picked from Tailings of 464-S2. Particle numbers 1, 2, 4 are the same as in Figure 52.

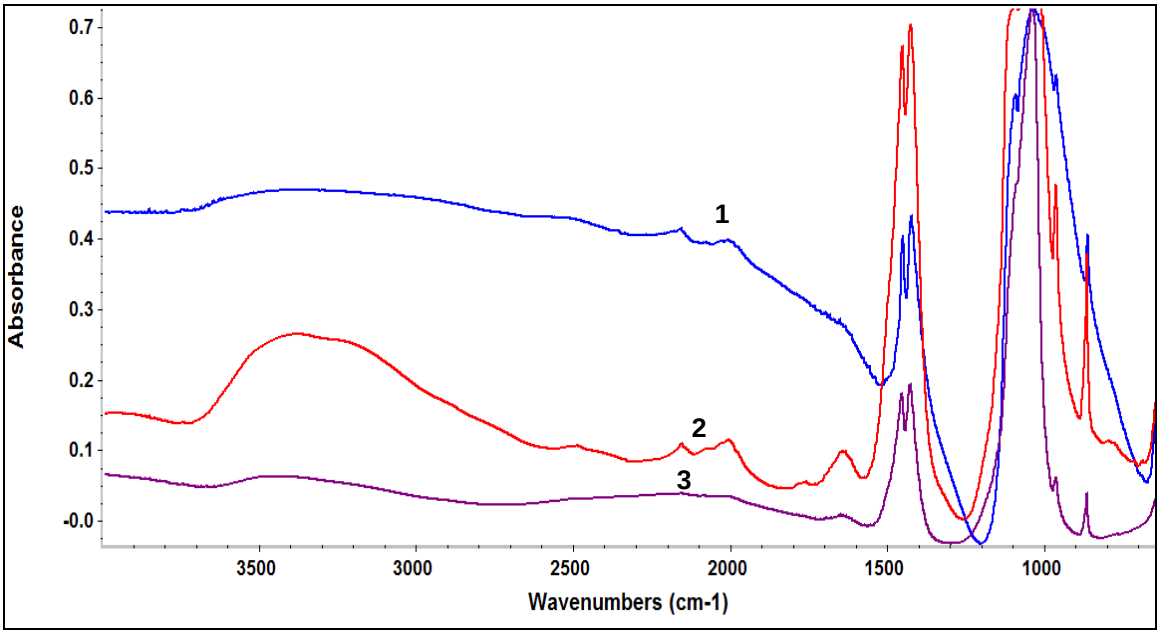

Figure 54. FTIR Transmission Spectra of Fine Black Particles Picked from Concentrate of 464-S2.

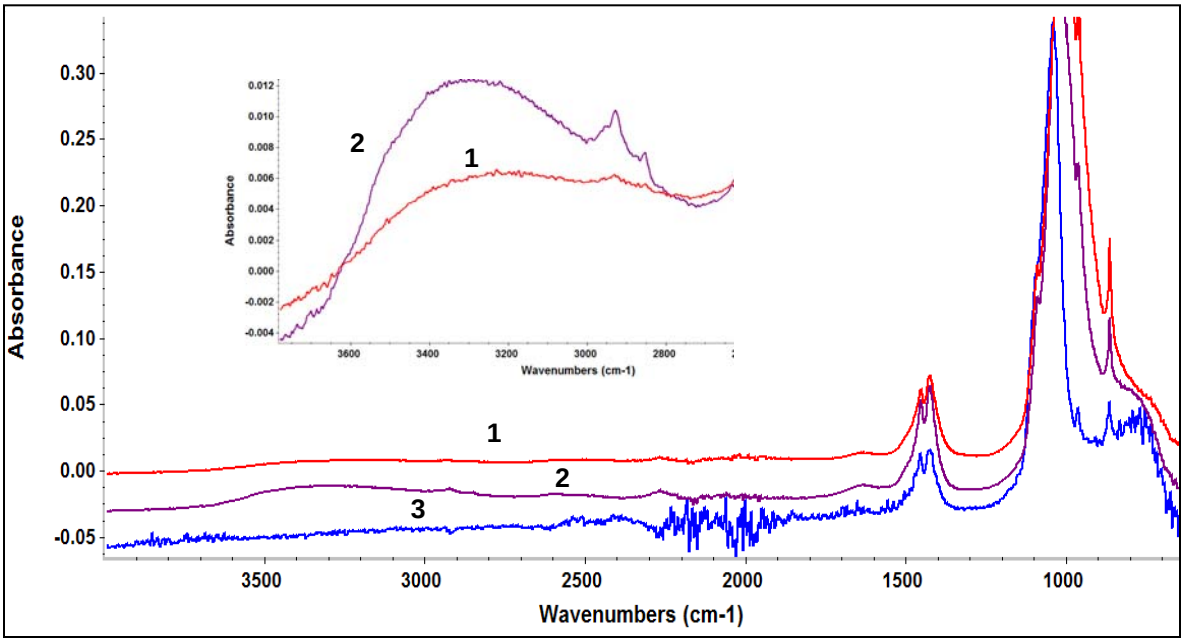

Figure 55. FTIR ATR Spectra of the Same Fine Black Particles Picked from Concentrate of 464-S2 as in Figure 54. Insert shows νCH region.

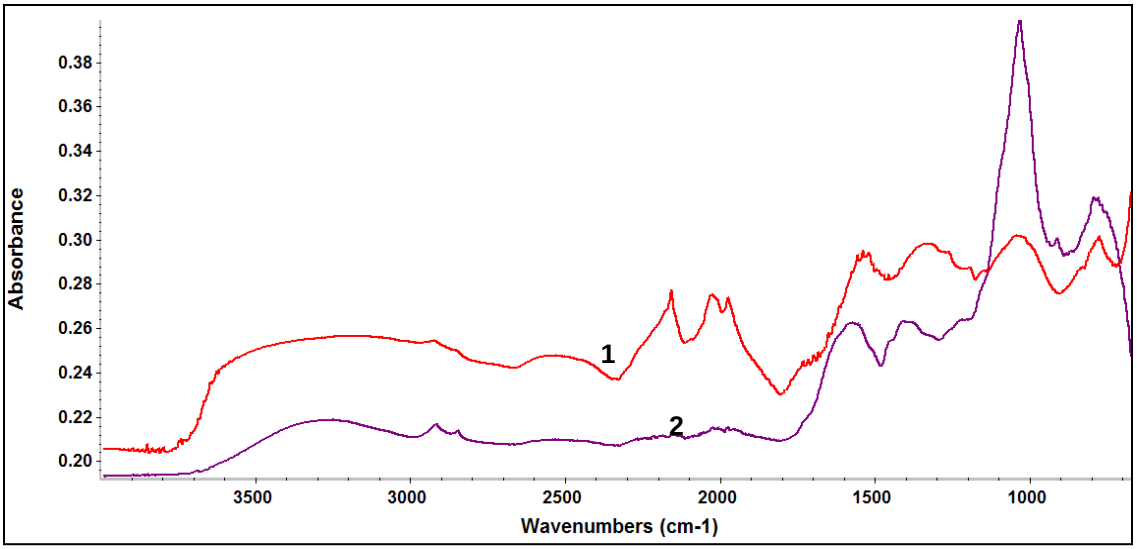

Figure 56. FTIR (1) Transmission and (2) ATR Spectra of the Same Fine Black Particle Picked from Tailing of SFM Sample.

The weak band at 3745 cm^{-1} due to surface silanol groups is observed in the ATR spectra of particles from the 3057-S2 tailings (Figure 30), which can be due to the presence of either quartz or silica-gel coating of the particles.

Finally, three of the four particles picked from FCO Bad tailings are characterized by a strong band at 840 cm^{-1} due to periclase (Figure 31), implying a higher fraction of the oxide in tailings compared to concentrate. Based on the FTIR data available and library spectra of minerals, there is no noticeable amount of dolomite and gypsum in tailings of all the three samples analyzed.

More FTIR transmission and ATR spectra of FCO Bad, CF West, 3057-S2, CF East, 464-S2 and SFM are shown in Figures 38-56. Transmission spectra are interpreted in Table 4. The presence of the PO_4 bands at ~1030 and 970 cm^{-1} in FTIR transmission and ATR spectra of all but one fine black particle studied testifies that hydroxyapatite/francolite is the main constituent of these particles. One black particle picked from tailings of 3057 was composed of quartz (#4 in Figure 42 and #2 in Figure 43).

On this basis, all the particles are referred to hereafter as 'phosphate' particles. The presence of aluminol groups in phosphate particles from FCO Bad (Figures 32 and 33) and 3057 **(**Figures 42 and 43) follows from the 3620-cm^{-1} band of the νAl_2OH vibrations, while the presence of silica tetrahedra follows from the two typical νSi-O vibrations at ~780 and 800 cm^{-1}. The bands are better resolved in the diffuse reflectance spectrum of FCO Bad tailings, which also reveal some amount of dolomite by the presence of shoulders on the CO_3 band (Figure 41, curve 1). It follows that, in agreement with the XRD results and similar to the case of coarse particles, these particles have a

certain amount of alumosilicates, with the maximum for particle 5 and minimum for particle 1 (Figure 38). Poor flotation recovery can be attributed to an admixture of alumosilicates.

Measurements of ATR spectra at several applied pressures revealed that the 800-cm^{-1} band tentatively assigned in the previous report to MgO (periclase) can be an artifact and, based on the XRD results, this possibility should be excluded. Comparison of transmission and ATR spectra measured on the same particle (Figure 40) does not reveal any compositional difference between the particle surface and bulk, which suggests that alumosilicate inclusions are distributed uniformly throughout the particle volume and are not accumulated at the surface.

Phosphate particles picked from the concentrate of CF West are composed mainly of hydroxyapatite/francolite without noticeable amounts of (alumino) silicates, as revealed by their transmission spectra (Figure 45). However, these particles have an admixture with dolomite. In fact, their transmission and ATR spectra (Figure 46) exhibit a shoulder at 880 cm^{-1} assignable to dolomite. In addition, ATR spectra have absorption bands at ~2900-3000 cm^{-1} due to νCH vibrations of adsorbed oleate. These bands are also present in ATR spectra of 464-S2 concentrate but are not observed in ATR spectra of phosphate particles from all tailings studied (Figures 39, 43, 48, 50, 51, 53), except for one particle from CF West (small intensity in curve 4, Figure 48). This fact implies that the degree of adsorption of the collector controls the floatability of phosphate particles: it is favored on phosphate particles from concentrates but is suppressed on those from tailings.

One of the four phosphate particles from tailings of the CF West sample (Figure 47, curve 2) is admixture with the bulk organic matter. This is distinguishable by strong absorption bands at ~2900 cm^{-1} due to CH groups, bands at 1740 cm^{-1} and 1550 cm^{-1} due to the νC=O and ν_{as}OCO– vibrations of molecular deprotonated and carboxylic groups, respectively, as well as by bands at 3290 and 1660 cm^{-1} due to the stretching (νNH) and bending (δNH) vibrations of molecular amine groups, respectively. Particles 3 (Figures 47-48) and 5 (Figure 48) have an admixture of alumosilicates, which can explain their occurrence in tailings. However, association with alumosilicate or organic matter is not considered to be the reason for the depression of particles 1 and 4. Their FTIR spectra (Figures 41-42) show no indication of these materials and are very similar to those of phosphates from concentrates of CF West (Figures 45-46). Since CF West tailings do not exhibit the oleate bands at 2900-3000 cm^{-1}, suppression of the collector adsorption could be assigned to degree of coating (compared to the phosphate in the concentrates) of phosphate particles with the organic phases.

Table 4. Comparison of FTIR Transmission Spectra Measured on Phosphate Particles Picked from Tailings of FCO Bad, 3057, 464-S2, CF West, CF East, and Concentrates of 464-S2 and CF West Samples.

Band Assigned	νSi–O in SiO4		δCO_3^{2-}	δAlOH	νPO_4	νCO_3^{2-}		δH_2O	νAl_2OH
WN, cm^{-1}	780	800	865	915	1030, 970	1425	1456	1620-1600	3620
FCO Bad Tails	775-780	795-800	865	Weak	+	1429	1455	1618, 1635,1,650	3615
	775-780	795-800	865	Weak	+	1429	1455	1618, 1635,1,650	N
	775-780	795-800	865	Weak	+	1429	1455	1618, 1635,1,650	3628, 3615
	775-780	795-800	865	Weak	+	1429	1455	1618, 1635,1,650	3628, 3615
	775-780	795-800	865	Weak	+	1429	1455	1618, 1635,1,650	3620
3057 Tails	771	Weak	866	N	+	1428	1453	1644,1655weak	N
	774	798	866	914	+	1424	1453	N	3620
	780	798	N	N	N	N	N	1655weak	N
	771	798	866	N	+	1428	1453	1644,1655weak	N
464-S2 Conc.	N	N	865	N	+	1430	1456	1642,1655	N
	N	N	864	N	+	1430	1456	1642weak,1655	N
	773	780	865	N	+	1430	1456	1642,1653	N
464-S2 Tail	N	N	865	N	+	1418	1453	1642,1650	3620
	777	798	865	N	+	1418	1453	1642weak,1650	3620
CF West Conc.	785	798	N	N	+	1427	1454	1645,1650	N
	781	N	N	N	+	1425	1454	1642,1650	N
	N	N	N	N	+	1428	1455	1643,1650	N
CF West Tails	N	N	N	N	+	1391	1452	1637,1653	3622
	779	797	N	923	+	1428	1455	1654,1653	N
	N	N	N	N	+	1428	1455	1643,1653	N
	N	N	N	N	+	1428	1455	1639,1653	3618
CF East Tails	778	798	N	Weak	+	1428	1455	1642,1653	3622
	778	798	N	Weak	+	1428	1455	1642,1653	3622

FTIR spectra of phosphate particles from tailings of CF East (Figures 50-51) show the presence of alumosilicates. As in the case of CF West, one of the four studied phosphate particles from tailings of 464-S2 has a lot of organic matter as an admixture (see curve 1 in Figure 52 and the discussion of curve 2, Figure 47 above). Particle 2 (Figures 52-53) has a significant amount of alumosilicates (bands at 3620, 800, 780 cm^{-1}) and an admixture of a metal (hydr)oxide, the presence of which is revealed by bands at 750 and 3700 cm^{-1} due to the νM–O and νOH vibrations, respectively. The other two particles bear alumosilicate inclusions (bands at 3620, 800, 780 cm^{-1}). Analysis of the dolomite band at 880 cm^{-1} shows that both tailings (Figure 52) and concentrate of 464-S2 (Figure 49) have an admixture of dolomite.

Transmission and ATR analysis of one black particle from SFM tailings (Figure 56) shows its main content is alumosilicates.

CONCLUSIONS FROM FTIR RESULTS

The FTIR microscopy study on coarse black particles picked from concentrate and tailings of three samples (CF East, 3057-S2, and FCO Bad) shows that:

- Except for one particle from FCO Bad tailing, all phosphate particles studied have isomorphically substituted carbonate groups typical of francolite.
- Phosphates in concentrates and tailings of CF East and 3057-S2 present carbonate-substituted apatites of varying stoichiometry and crystallinity. However, this may not be the determining factor for the floatability of the particles studied.
- Presence of periclase (MgO) inclusions is typical for both concentrates (1 of 3 particles) and tailings (3 of 4 particles) of FCO Bad sample.
- Tailings of CF East differ from concentrate by a higher amount of acidic surface Al–OH–Al and SiOH groups and alumosilicate inclusions.
- Particles from 3057-S2 tailings have surface silanol groups, which may explain their depression.
- Black fine and coarse particles from tailings of the FCO Bad sample as well as fine black particles picked up from tailings of the 1862 and 3057 samples are composed of francolite and carbonate hydroxyapatite with an admixture of calcium carbonate hydrate and different calcium aluminum silicate hydrates and magnesium aluminum silicates. 3057 and FCO Bad samples have a small admixture of dolomite. FCO Bad and 1862 samples have a significant admixture of quartz.
- Dolomite is associated with both concentrate and tailings.
- Unliberated or finely disseminated phosphate in alumosilicates is one of the main reasons for loss of phosphates to tailings.
- The above conclusion is strengthened by the fact that alumosilicate inclusions are distributed uniformly in the bulk of the phosphate particles, and, particularly, the aluminosilicates are not accumulated at the surfaces.

- CF West and 464-S2 include organic matter, which may contribute to processing problems as well as affect final product quality. The main result of its presence could be a lack of adsorption of collector onto the phosphate particles.
- There is an additional source of depression for CF West, which should be further studied. Phosphate grains from its tailings are partially coated by organic matter.

CONCLUSIONS

EDX

Based on EDX and FTIR data, francolite is present in the particles studied. Along with the francolite, the possible presence of aluminosilicates/alumina and magnesium-containing mineral is also suggested.

XRF

A high Ca content was shown in the bad feed samples (1862-S1). The results with 464-S1 showed a higher Ca content on concentrate samples than that on either feed or tailings.

ADSORPTION

Adsorption of collector was observed to be slightly higher on good feed samples (EF east, FCO Good) than on bad feed samples (1862-S1 and 464-S1).

XRD

Phosphate particles in the tailing samples show admixtures of different types of Ca/Mg aluminosilicates, clay-type minerals, dolomite and quartz. XRD of white particles confirm that they are quartz, but these samples have phosphate mineral phases associated with them.

FTIR

The FTIR microscopy study on coarse black particles picked from concentrate and tailings of three samples (CF East, 3057-S2, and FCO Bad) shows that:

(1) Except for one particle from FCO Bad tailing, all phosphate particles studied have isomorphically substituted carbonate groups typical of francolite.
(2) Phosphates in concentrates and tailings of CF East and 3057-S2 present carbonate-substituted apatites of varying stoichiometry and crystallinity. However, this may not be the determining factor for the floatability of the particles studied.
(3) The presence of periclase (MgO) inclusions is typical for both concentrate (1 of 3 particles) and tailings (3 of 4 particles) of the FCO Bad sample.
(4) Tailings of CF East differ from concentrate by a higher amount of acidic surface Al–OH–Al and SiOH groups and alumosilicate inclusions.
(5) Particles from 3057-S2 tailings have surface silanol groups, which may explain their depression.
(6) There is no noticeable amount of dolomite and gypsum in tailings of all the three samples analyzed.

Table 5. Differences Between Good and Bad Samples from EDX, XRF, Zeta Potential, XRD and FTIR Results.

	Good Phosphate Samples	Bad Phosphate Samples
Elemental Analysis (EDX and XRF)	CF East Feed Good flotation attributed to significant liberation of phosphates particles	FCO Bad Poor flotation due to poor liberation of phosphate particles 1862-S2, 464-S1
Adsorption Studies	At higher dosages of sodium oleate, adsorption on the feed sample CF East & FCO (5-07) is HIGHER.	At higher dosages of sodium oleate, adsorption on the feed sample 1862-S1 & 464-S1 is LOWER.
Zeta Potential Studies	CF East, CF Combined and FCO (5-07) showed negative zeta potential which is generally observed for silicates	1862-S2 feed showed comparatively less negative zeta potential than for good samples
XRD Studies		FCO Bad, 1862 and 3057 phosphate particles have aluminosilicates and clay type minerals as inclusions. FCO Bad quartz samples show phosphate inclusions in them.
FTIR	CF East Surface of coarse phosphate particles from tailings has acidic (aluminol and silanol) groups. Since even bad feed (3057-S2) also showed presence of silanol/aluminol groups on the surface, it can be hypothesized that the presence of such phosphate particles (with silanol inclusion) is lesser in the good samples than in the bad samples as can be interpreted from flotation data. This hypothesis needs to be further tested.	1862-S2 • Periclase dominates on the surface whereas francolite is in the bulk • Surface enriched with Silanol groups Poor liberation of francolite and poor adsorption of collector on the phosphate particles is due to acidic surface (silanol group) are the reasons for low recovery of phosphate FCO Bad Samples • Isomorphic substitution of carbonate groups • Higher fraction of interlocked oxide in the tailing samples compared to concentrate Poor liberation of francolite can be a reason for low recovery of phosphate 3057 • Presence of surface silanol groups Poor adsorption of collector on the phosphate particles is due to acidic surface (silanol group) are the reasons for low recovery of phosphate

Table 6. Differences Between Concentrate and Tails.

	Concentrate	Tailings
Elemental Analysis (XRF)	CF East, FCO Bad, 1862-S2 and 464-S1 High Ca elemental concentration observed compared to feed	CF East, FCO Bad, 1862-S2 and 464-S1 Low Ca elemental concentration observed compared to feed
Surface and Bulk Analysis with FTIR	CF East, 3057, FCO Bad CF East • Phosphate particles (apatite) showed varying degree of stoichiometry and crystallinity. FCO Bad • Phosphate particles exhibited concentration of periclase inclusions (1 out of 3 particles analyzed) 3057 • Phosphate particles (apatite) showed varying degree of stoichiometry and crystallinity	CF East, 3057, FCO Bad, 1862-S2 CF East • Phosphate particles show higher amount of acidic surface (Al-OH-Al groups, SiOH and Aluminosilicates inclusions) FCO Bad • Phosphate particles show high concentration of periclase inclusions (3 out of 4 particles analyzed). Except for one particle phosphate particles have isomorphically substituted carbonate groups. 3057-S2 • Phosphate particles showed surface silanol groups 1862-S2 • Surface of phosphate particles are enriched with oxide and silanol groups

REFERENCES

Matthews A, Nathan Y. 1977. The decarbonation of carbonate-fluorapatite (francolite). American Mineralogist 62(5-6): 565-73.

Panda RN, Hsieh MF, Chung RJ, Chin TS. 2003. FTIR, XRD, SEM and solid state NMR investigations of carbonate-containing hydroxyapatite nano-particles synthesized by hydroxide-gel technique. Journal of Physics and Chemistry of Solids 64(2): 193-99.

Paschalis EP, DiCarlo E, Betts F, Sherman P, Mendelsohn R, Boskey AL. 1996. FTIR microspectroscopic analysis of human osteonal bone. Calcified Tissue International 59(6): 480-7.

Pleshko N, Boskey A, Mendelsohn R. 1991. Novel infrared spectroscopic method for the determination of crystallinity of hydroxyapatite minerals. .Biophysical Journal 60(4): 786-93.

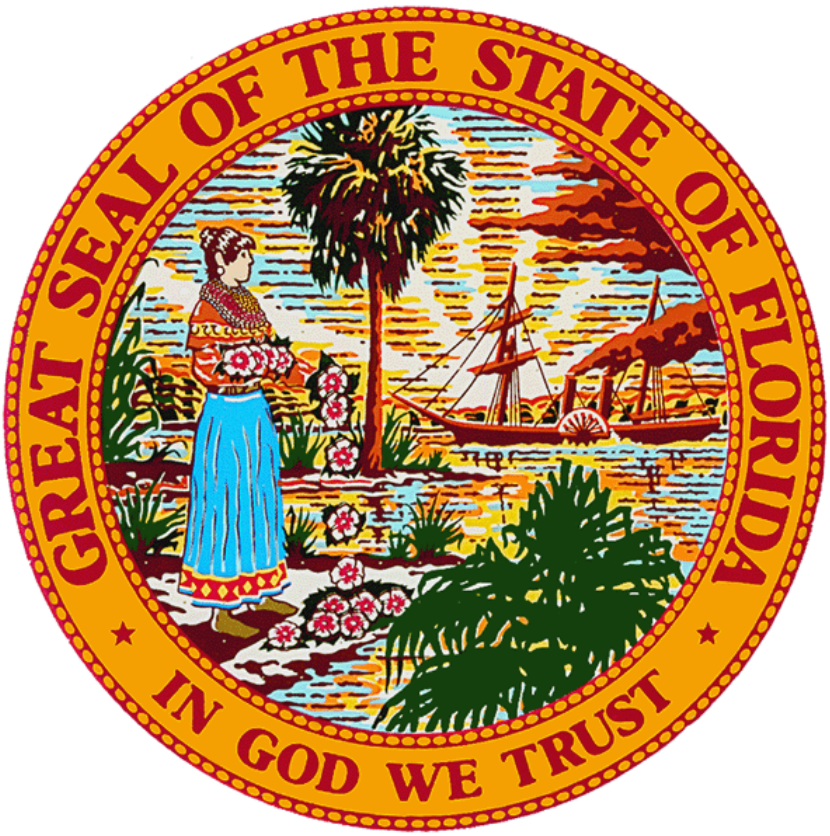
GREAT SEAL OF THE STATE OF FLORIDA
IN GOD WE TRUST